

A NEW FISSION-GAS RELEASE MODEL

R.J. WHITE and M.O. TUCKER

Central Electricity Generating Board, Berkeley Nuclear Laboratories, Berkeley, Gloucestershire, GL13 9PB, UK

Received 21 February 1983; accepted 14 April 1983

The release of unstable fission products from irradiated UO_2 fuel is shown to be a sensitive function of many inter-related factors. The poly-granular-aggregate model for unstable gas release assumes that the release of fission products from the interior regions of UO_2 fuel occurs, firstly, by direct diffusion to grain boundaries and, secondly, by gaseous diffusive transfer through an intermittently open grain-edge tunnel network.

During the early stages of irradiation a saturated network of grain-face lenticular porosity is established by the precipitation of stable fission-gas atoms. Lenticular bubbles which nucleate near to the grain edges—junctions of the three grains—will move to a lower free energy configuration on those edges and take up a triangulated cigar shape. Continued stable gas collection inflates these bubbles to a point of interlinkage beyond which point the fission gases are vented and tunnel collapse, by means of surface diffusion away from regions of high curvature, into a string of cigar-shaped bubbles occurs.

This process is repeated many times until the resulting grain-edge tunnel “pinches off” in the centre of the tunnel resulting in bubbles at the grain corners—the junction of four grains. The re-inflation of these grain-corner bubbles—tetrahedra with spherical faces—results in a permanently interlinked network of tunnels which are unconditionally stable and can resist further collapse. Using simple arguments, we demonstrate that the interlinkage times for bubble strings and the pinch-off times for tunnels effectively delay the passage of fission products from the fuel interior to the exterior and that this mechanism may be viewed as an effective diffusion process.

The arrival rate of atoms into the tunnel network may be by direct diffusion or indirectly from the grain-face lenticular porosity. In the latter case some radioactive decay may have occurred, depending on the length of time spent in that porosity. The nett arrival rate into the grain-edge or corner porosity—both direct and indirect—is treated as an effective generation rate. Because the swelling rate of fuel depends on this growth and collapse of porosity it is clear that the swelling rate and hence ultimately the release rate of unstable fission products depends critically on the stable fission-gas release. In turn, the release of stable fission gases depends on the irradiation-induced resolution-controlled diffusion from the UO_2 grains.

A model incorporating the Speight-Turnbull stable gas release model, the grain edge-corner swelling model and the Tucker-White percolation diffusion model from a polygranular aggregate is shown to account well for the experimental findings of Turnbull and Friskney on release rates of I^{131} , I^{133} , Xe^{133} , Xe^{138} , Kr^{88} from 1.46% enriched stoichiometric UO_2 . It is shown that uncertainties in ratings of $\pm 5\%$ and in fuel temperature of $\pm 25^\circ\text{C}$ are unlikely to seriously limit the accuracy of the predictions for unstable release rates, and it is proposed that the model be used to reinterpret the Turnbull-Friskney experiments to yield “second generation” estimates of diffusion coefficients.

CONTENTS

1. Introduction
2. Outline of the model
3. Diffusional release from idealized spherical grain
4. Diffusion coefficients and intra-granular porosity
 - 4.1. The single gas atom diffusion coefficient
 - 4.2. The effect of trapping at intragranular porosity on the fission-gas diffusion coefficients
 - 4.3. Evaluation of trapping parameters
5. Inter-granular porosity and irradiation-induced resolution
 - 5.1. Geometric considerations
 - 5.2. Approach to saturation-limitation by irradiation-induced resolution
 - 5.3. Post-incubation release

6. The release of unstable fission products

6.1. Transient release

6.2. Effect of irradiation-induced resolution:

(a) from intragranular porosity,

(b) from grain-boundary porosity

6.3. Effect of unstable atom delay at grain face porosity

7. Development of grain-edge and corner porosity

7.1. The toroid model for edge porosity

7.2. Kinetic development of edge porosity

7.3. Kinetic development of corner porosity

7.4. Swelling above stable tunnel interlinkage

8. The poly-granular aggregate (PGA) model for unstable gas release

8.1. Model concept

8.2. Direct loss from outer geometric free surface of PGA

8.3. The effective generation rate

8.4. The effective diffusion coefficient for gas release by way of percolation through the grain-edge tunnel network

9. Parameter values

9.1. General

9.2. Well characterised parameters

9.3. Less well characterised parameters

9.4. Complete experimental unknowns

10. Parametric comparison

10.1 Philosophy

10.2. Stable gas release

10.3. Grain-edge swelling

10.4. Unstable release

10.5. Effects of variation of the bubble spacing parameters

10.6. Effects of variation of the pinch-off proportionality parameter

10.7 Summary

11. Experimental results

11.1. The data

11.2. The simulations

12. Conclusions

Appendix 1.

A1.1. The mean dwell time at grain corners

A1.2. The mean jump distance along interconnected porosity network

A1.3. The mean time between complete corner re-opening

Appendix 2. Geometrical relationships for porosity

Appendix 3. Fuel swelling after tunnel interlinkage ($\Delta V/V > 6\%$)

Appendix 4. Irradiation history for Turnbull & Friskney experiments

Appendix 5. List of symbols

References

1. Introduction

The release of the stable fission gases, xenon and krypton, from irradiated UO_2 nuclear fuel is an inevitable consequence of the insolubility of these gases in UO_2 . The rate of release is generally attributed to an atomic diffusion process to the grain boundaries of the material.

Under ideal conditions the fuel cladding material is in intimate thermal contact with the fuel, thus ensuring rapid heat transfer. The release of gaseous fission prod-

ucts can lead to a variety of unwelcome effects; for example, the effect of the gas pressure may reduce the degree of contact at the cladding/fuel interface, thus reducing the heat transfer from fuel to coolant. Since the fission gas diffusion process is strongly temperature-dependent, any increase in fuel temperature may exacerbate the situation and eventually lead to cladding failure.

Perhaps a more important problem from the viewpoint of radiological safety is the content of radioactive gases and volatile solids present in the pin at any stage.

In the event of fuel pin failure the release of I^{131} would present a considerable health hazard, particularly if accompanying or occurring as a result of a serious reactor fault condition such as depressurization (in the case of AGR) or loss of liquid coolant in a water reactor situation.

In view of the deleterious nature of fission-gas release it is essential to be able to estimate the amount of extragranular fission gas inside the pin at any stage of the irradiation. This of course requires a detailed knowledge of the fuel pin history in terms of temperature, rating, etc., a history which we will assume, for the purposes of this paper, to be well characterised.

In this paper we propose an improved model for the description of fission-gas and unstable fission-product release. The approach is essentially a development of the diffusional release model adopted in the MINIPAT code [1] but the release of unstable fission products is controlled here by the development of the grain-edge swelling process in UO_2 .

The experimental work of Turnbull and co-workers is central to the calibration of this particular model and their results for the five isotopes Xe^{138} , Kr^{88} , Xe^{133} , I^{133} and I^{131} (with half-lives varying from 14 minutes to 8 days) are used for the purpose of calibration.

2. Outline of the model

The release of fission products from irradiated fuel is generally considered to be controlled by atomic diffusion to the fuel grain boundaries. The pioneering work of Booth [2] is the starting point for most diffusion-based interpretations, but the overall picture is somewhat confused by the fact that UO_2 fuel consists of a sintered compact of granular UO_2 and ultimate release from the fuel may occur much later than the Booth calculations on single grains would indicate. The Booth approach has thus been modified by subsequent workers in the field (Speight [3], Turnbull [4]) and whilst the overall "spirit" of the model has been retained, the agreement with experiment has been considerable improved. The following summarises the main improvements in the diffusion-based interpretation.

(a) Intragranular porosity

After a short irradiation period there develops a fine intragranular dispersion of small bubbles ($r \approx 10^{-9} m$). Under any particular set of conditions, rating, temperature etc., this porosity rapidly stabilizes in such a way that the size and concentration of bubbles remains invariant under further irradiation [5,6]. Turnbull [7] has shown that this equilibrium situation is understandable

if the bubbles are considered to be heterogeneously nucleated in the wake of energetic fission fragments where they grow by collecting fission gas before being destroyed by the passage of another fission fragment. Speight [8] has further refined Turnbull's calculations by describing how such a process may result in a reduced effective gas-atom diffusion coefficient.

(b) Intergranular porosity

Scanning electron micrographs of the fractured surfaces of irradiated UO_2 fuel show the grain boundaries to be decorated by large (micron-sized) lenticular bubbles. It has been observed that the onset of stable fission gas release is generally delayed until the grain-boundary porosity attains a value equivalent to the fuel swelling of $\sim 3\%$. Manley [9] has shown that the development of the grain-boundary swelling is strongly influenced by irradiation-induced resolution processes and Speight [3] has given an analytic description of such a process. The "saturation" of the grain boundaries in reality constitute an "incubation" time for the onset of fission-gas release. Turnbull [4] has also shown that the subsequent release of fission gases from the saturated grain faces may be described by the Booth equations if due account is taken of the resolution process at the grain boundary.

After the "incubation time" referred to in (b), fission gases are observed to "seep" out of the fuel and in the case of stable atoms the subsequent delays imposed by closed grain-edge porosity are immaterial since no loss by decay occurs during these "storage" periods. In the case of radioactive products this delay is, of course, vitally significant. The release of unstable fission products to the fuel pin interior is considered to be delayed by two main processes and these have been described by Tucker & White [10]. The first process is the delay in closed lenticular boundary porosity and is assumed to be dependent on the arrival rate of stable gas atoms to the boundaries. The second process is a result of the progressive development and collapse of grain-edge * porosity. This porosity is of course itself critically dependent on the arrival rate of stable gas atoms but the important feature of the Tucker & White description is the development of an effective diffusion coefficient to model the release of unstable products from the sintered compact. The evaluation of this diffusion coefficient requires an understanding of the bubble swelling and tunnel collapse processes.

* By *grain edge* we mean the region where three grains meet; this region has approximate threefold symmetry.

3. Diffusional release from idealised spherical grain

Booth [2] treats the release of fission gases from the UO_2 as a diffusion process to the surface of a spherical grain. Although the grains in UO_2 are not spherical this approach has many attractions, not least among them being simplicity. It is a simple matter to relate the tetra-kaidecahedral or truncated octahedral grains of UO_2 to an equivalent sphere by equating the volumes and this is to be preferred since any alternative definitions, say ratios of surface area to volume, are likely to change during the course of the irradiation process.

The Booth treatment of gas release assumes that gas is created uniformly throughout a grain of radius "a" at a rate β . The diffusion equation which must be satisfied at all points within the sphere is

$$\frac{\partial c}{\partial t} = D \nabla^2 c + \beta, \quad (1)$$

subject to $c = 0$ at $r = a, 0 \leq t;$
 $0 \leq r \leq a, t = 0;$

and $\frac{\partial c}{\partial r} = 0$ at $r = 0,$

the last requirement being simply for symmetry. The quantity released after time t may be calculated by integrating the divergent flux across the specimen boundary up to time t or by integrating the concentration profile. Both methods yield the same result for the fractional release, f_c ,

$$f_c = 1 - \frac{6}{\omega} \sum_{n=1}^{\infty} \frac{1 - \exp(-\pi^2 n^2 \omega)}{(n\pi)^4} \quad (2)$$

with $\omega = Dt/a^2$.

For short times $\omega < \pi^{-2}$, when eq. (2) is approximately given by

$$f_c = 4 \left(\frac{\omega}{\pi} \right)^{1/2} - \frac{3}{2} \omega, \quad (3)$$

which is valid for fractional releases up to 57%. Beyond this value of release the expression

$$f_c \approx 1 - \frac{0.0662}{\omega} \{ 1 - 0.93 \exp(-\pi^2 \omega) \} \quad (4)$$

may be used.

Eqs. (2)–(4) describe the diffusional release of stable gases from a sphere of UO_2 when the initial concentration throughout the grain is zero. There are occasions when the generation of fission gases may cease but the temperature remains sufficiently high for previously generated fission products to continue diffusing across the fuel boundaries. Booth [2] also treats this problem of "post-irradiation annealing". In this case β in eq. (1)

is set to zero and the initial concentration throughout the grain is set to C^0 and assumed uniform everywhere. Strictly speaking a concentration profile, equivalent to that existing at the end of the irradiation period, should be used but for clarity we follow the simpler Booth treatment. Schilling [11] treats the post-irradiation annealing situation more rigorously.

The fraction released on annealing, f_A , is that fraction of the initial concentration of atoms ($4\pi a^3 C^0/3$) which have escaped at time t or ($\omega = Dt/a^2$).

$$f_A = 1 - \frac{6}{\pi^2} \sum_{n=1}^{\infty} \frac{\exp(-\pi^2 n^2 \omega)}{n^2} \quad (5)$$

and the series converges rapidly at long time, $\omega > \pi^{-1}$, to

$$f_A = 1 - \frac{6}{\pi^2} \exp(-\pi^2 \omega). \quad (6)$$

At short times, $\omega < \pi^{-2}$, eq. (5) is approximately given by

$$f_A = 6 \left(\frac{\omega}{\pi} \right)^{1/2} - 3\omega. \quad (7)$$

Eqs. (6) and (7) may be used for fractional annealed releases above and below 77%, respectively.

4. Diffusion coefficients and intragranular porosity

4.1. The single gas atom diffusion coefficient

The release processes of both stable and unstable fission products are assumed to be primarily controlled by atomic diffusion through the UO_2 lattice. The first stage of release is assumed to be to the UO_2 grain boundaries. There may be several delaying processes occurring between generation and arrival at grain boundaries, as we have seen in section 2, but it is essential to have at hand an analytical description of the single gas atom diffusion coefficient. This description must include the temperature (and rating) dependence of the diffusion process.

The eventual release rate will of course reflect any trapping at intragranular porosity, but we confine our attention here to the diffusion rate in the absence of these delaying mechanisms. In a series of papers, Turnbull & Friskney [12], Friskney & Turnbull [13] and Turnbull et al. [14] have studied the releases of a variety of unstable fission products over a wide range of temperature both in small- and large-grain aggregates and in single crystals. Their work has culminated in the provision of a partly physically based analytic expres-

sion for the diffusion coefficient of single gas atoms in UO_2 . The diffusion process is concluded to be controlled in different temperature ranges by at least one of three distinct mechanisms.

At the highest temperatures an "intrinsic" thermally activated process appears to dominate, although this is not fully understood. This contribution has a temperature dependence similar to that reported by Davies and Long [15],

$$D_1 = 7.6 \times 10^{-10} \exp(-3.03/kT) \text{ m}^2/\text{s} \quad (8)$$

and it seems likely that the mechanism is one of gas diffusion through the cation lattice by means of thermally activated vacancies. Below 1400°C, Turnbull et al. [14] conclude that diffusion occurs by means of vacancies produced by the irradiation process. Since interstitials are produced in equal numbers with these vacancies, a certain amount of vacancy loss occurs both by capture at fixed sinks such as gas bubbles, grain boundaries and dislocations and by mutual recombination with interstitials.

We write the vacancy and interstitial concentrations as C_V and C_I , respectively, and using the Rate Theory Continuum model for a point defect behaviour, Brailsford & Bullough [16], we obtain

$$\left. \begin{aligned} \frac{dC_I}{dt} &= K - D_V C_V k_V^2 - \alpha C_I C_V \\ \frac{dC_V}{dt} &= K - D_I C_I k_I^2 - \alpha C_I C_V \end{aligned} \right\} \quad (9)$$

K is the displacement rate of atoms from their lattice sites per second. The second term is the diffusional flow of defects to fixed internal sinks, k^2 , where a distinction between vacancy and interstitial sink strength results from the "biased" nature of the dislocation [17]. The last term in eq. (9) describes the mutual annihilation process of vacancy meeting interstitial, and $\alpha = ZD_1/S^2$, where Z is the number of sites around a defect from which mutual recombination is inevitable. S is the atomic jump distance.

The solutions of eq. (9) may be obtained in the steady-state situation and yield (for $dC_\alpha/dt = 0$)

$$C_\alpha^0 = \frac{KF(\eta)}{D_\alpha k_\alpha^2} \Bigg|_{\alpha=I,V.} \quad (10)$$

where

$$F(\eta) = \frac{2}{\eta} \left\langle (1 + \eta)^{1/2} - 1 \right\rangle, \text{ with } \eta = \frac{4KZ}{k_V^2 k_I^2 D_V S^2}.$$

We shall see later that the dominant sink k_α^2 is a fine dispersion of intragranular gas bubbles and these are

assumed to be "unbiased", that is, they exert no particular preference for interstitials or vacancies. The vacancy mobility D_V may be related to the vacancy jump frequency j_V using the standard random walk arguments $D_V = S^2 j_V$ and the resulting contribution to the fission gas diffusion coefficient will be of the form

$$D_2 = S^2 j_V C_V^0, \quad (11)$$

with

$$C_V^0 = \frac{k_I^2 S^2}{2Z} \left\{ \left(1 + \frac{4KZ}{j_V k_V^2 k_I^2 S^4} \right)^{1/2} - 1 \right\}.$$

The damage rate K refers to the displacement rate of atoms from their lattice sites during irradiation. Turnbull estimates that the yield of point defects lies somewhere between 10^4 and 5×10^5 defects per fission event. If the fission rate is $F(\text{m}^{-3}\text{s}^{-1})$ and the atomic volume Ω , then

$$10^4 F\Omega \leq K \leq 5 \times 10^5 F\Omega.$$

The jump distance $S = \Omega^{2/3}$ and jump frequency of the vacancy

$$j_V \sim 10^{13} \exp(-2.39/kT).$$

Turnbull reports that somewhat better agreement is found with the higher yield of vacancies ($\sim 5 \times 10^5$) per fission event.

The final contribution to the diffusivity is the "athermal tail" and no firm conclusions emerge as to the mechanism. Turnbull follows Matzke [18] in adopting a term proportional to the fission rate and scaled to agree with the low temperature plateau. This he writes

$$D_3 = 2 \times 10^{-40} F \text{ m}^2/\text{s} \quad (12)$$

and the total single gas atom diffusivity as

$$D = D_1 + D_2 + D_3. \quad (13)$$

4.2. The effect of trapping at intragranular porosity on the fission gas diffusion coefficients

It is commonly observed [5] that after a short period of irradiation the intragranular structure of UO_2 is decorated by a population of small ($r \sim 10^{-9} \text{ m}$) bubbles. This gas bubble population rapidly stabilizes in both size and number density and this apparent "stasis" has prompted several analyses. Before discussing the Turnbull [7] resolution model in detail we propose to outline the phenomenological treatment of Speight [3].

Speight considers the diffusion of fission gas atoms from a spherical grain of UO_2 which contains a fixed number of saturable traps. The gas in the traps is

labelled "m" to distinguish it from the matrix or dissolved gas "c". Absorption of the matrix gas into the traps takes place at a rate g and resolution, from the trap back into the matrix, at a rate b' . Thus the diffusion equation may be written

$$\frac{\partial c}{\partial t} = D \nabla^2 c - gc + b'm + \beta, \quad (14)$$

where β is the generation rate. The time dependence of the trapped gas is described by

$$\frac{\partial m}{\partial t} = gc - b'm. \quad (15)$$

Speight seeks accurate time-dependent solutions to the pair of eqs. (14) and (15). The overall behaviour of the system may however be judged by writing the total gas concentration as

$$\psi = c + m \quad (16)$$

and noting that for times greater than $5b'^{-1}$ the traps are effectively saturated, giving $\partial m / \partial t = 0$. Therefore we may rearrange eqs. (14) and (15), subject to these two assumptions, to yield

$$\frac{\partial \psi}{\partial t} = \frac{Db'}{b' + g} \nabla^2 \psi + \beta, \quad (17)$$

which is the equation solved by Booth [2], eq. (1), for the standard treatment of gas release.

Eq. (17) indicates that the Booth [2] treatment is valid in the presence of saturable traps but with an effective diffusion coefficient defined by

$$D' = Db' / (b' + g). \quad (18)$$

4.3. Evaluation of the trapping parameters

In section 4.2 we have seen how the presence of saturable traps modifies the gas release by reducing the diffusion rate of fission gas atoms. The model proposed and later improved by Turnbull [7,19] enables us to calculate b' and g and hence to calculate the effective diffusion coefficient.

In order to explain the invariance of the bubble population, Turnbull [7] proposes that bubbles are nucleated in the wake of energetic fission fragments and that each fragment can nucleate α bubbles. We have therefore 2α bubbles created for every fission. These bubbles grow by a diffusion limited process and are eventually destroyed by the passage of another fission fragment. Turnbull [19] assumes that a fission fragment has a range of influence about its path of Z_0 , where $Z_0 = 10^{-9}$ m, and that a single "graze" or collision is sufficient to totally destroy the bubble.

It is further assumed that the fragment travels a distance $l_f = 6 \times 10^{-6}$ m [20] before coming to rest. The path of the fission fragment therefore destroys all bubbles of radius R whose centres are within $R + Z_0$ of the centre of the fission fragment path. If the total density of bubbles is C_B^{tot} , the destruction rate of bubbles is $2\pi Fl_f(R + Z_0)^2 C_B^{\text{tot}}$ and we may therefore write

$$\frac{dC_B^{\text{tot}}}{dt} = 2Fl_f(R + Z_0)^2 C_B^{\text{tot}}. \quad (19)$$

Eq. (19) indicates that the bubble concentration should eventually saturate at the value

$$C_B^{\text{tot}} = \frac{\alpha}{\pi l_f(R + Z_0)^2} \quad (20)$$

and the observations of Baker [21] indicate that this is indeed so with $\alpha = 24 \pm 2$ bubbles generated per fission and $Z_0 \approx 10^{-9}$ m (table 1).

The Speight [8] analysis for calculation of bubble size distribution may be modified in the light of eq. (19) and for this particular resolution mechanism yields

$$C_B(R) = \frac{2F\alpha R}{bDc} \exp \left\{ \frac{-2F\pi l_f}{bDc} \left[\frac{R^4 - R_0^4}{4} + \frac{2Z_0}{3}(R^3 - R_0^3) + \frac{Z_0^2}{2}(R^2 - R_0^2) \right] \right\} \quad (21)$$

where b is the Van der Waals constant for the gas (mainly xenon), c the fission gas concentration in solution in equilibrium with the bubble population, R_0 is the nucleation radius of freshly created bubbles.

Examination of eq. (21) suggests that the single gas atom diffusion coefficient D may be calculated from detailed measurement of the bubble population. Observations are made of the most probable bubble size R^* and the condition for this may be obtained by differentiating eq. (21) and equating to zero.

$$\frac{dC_B(R)}{dR} = 0, \quad \text{when } D = \frac{2\pi Fl_f R^{*2} (R^* + Z_0)^2}{cb} \quad (22)$$

and care must be exercised since $R^* \neq \bar{R}$. However, the values of D obtained by using eq. (22) fall considerably below those predicted from eqs. (8) and (11)–(13); the primary reason for the discrepancy must be in the evaluation of c , the intragranular gas atom concentration. Baker [21] calculates that the fraction of gas in bubbles at 1800°C is ~35%, whereas a calculation based on observed bubble size and densities indicates that the amount exceeds the entire generated inventory. Thus there must be an associated uncertainty in the fission rate. To avoid these uncertainties we assume the diffusion coefficient to be that calculated in eqs. (8) and

Table 1
After Baker [21]

Temp. (°C)	Bubble		$D^a)$ [19] (m ² /s)	$Db'/(b'+g)$ (m ² /s)	Number of bubbles per fission α
	Radius ($\times 10^{-10}$ m)	Density ($\times 10^{23}$ m ⁻³)			
1000	5.5	8.7	7.98×10^{-21}	7.70×10^{-21}	25.9
1100	6.0	7.8	1.46×10^{-20}	1.37×10^{-20}	24.8
1200	6.5	7.0	4.49×10^{-20}	3.82×10^{-20}	23.6
1300	7.0	6.4	1.74×10^{-19}	1.06×10^{-19}	22.9
1400	8.0	5.7	6.32×10^{-19}	2.02×10^{-19}	22.9
1500	8.75	5.3	2.04×10^{-18}	2.78×10^{-19}	23.1
1600	9.75	4.8	5.83×10^{-18}	3.32×10^{-19}	23.2
1700	11.0	4.4	1.50×10^{-17}	3.76×10^{-19}	24.1
1800	12.5	3.8	3.53×10^{-17}	4.22×10^{-19}	23.8

^{a)} Calculated from eqs. (8), (11)–(13).

(11)–(13) and use the observations of Baker [21] to calculate an attenuation coefficient.

The evaluation of b' requires caution because of the bubble size distribution and we choose to define it as follows

$$b' = 2\pi Fl_f (\bar{R} + Z_0)^2 \times \frac{\int_0^\infty C_B(R)(R + Z_0)^2 R^3 dR \int_0^\infty C_B(R) dR}{\int_0^\infty C_B(R)(R + Z_0)^2 dR \int_0^\infty R^3 C_B(R) dR}. \quad (23)$$

Using the distribution in eq. (21) we obtain from numerical integrations with $R_0 = 0$ and $Z_0 = 10^{-9}$ m,

$$b' = 3.03Fl_f (\bar{R} + Z_0)^2. \quad (24)$$

The capture rate at bubbles g is given by Ham [22] as

$$g = 4\pi\bar{R}C_B^{\text{tot}}D. \quad (25)$$

For the gas atom concentrations within and without bubbles steady state conditions are reached with $\partial m/\partial t = 0$ in eq. (15). This occurs when $b'm = gc$ and since m is the total concentration of gas in bubbles

$$3.03Fl_f (\bar{R} + Z_0)^2 \frac{4}{3} \frac{\pi\bar{R}^3}{b} C_B^{\text{tot}} = 4\pi\bar{R}C_B^{\text{tot}}Dc. \quad (26)$$

The bubble size distribution in eq. (21) yields $\bar{R}^3 = 1.636\bar{R}^3$ and using this result, eq. (26) reduces to a similar form to eq. (22).

For analytical purpose we have chosen to describe Baker's bubble size and density by the following:

$$\bar{R} = 5 \times 10^{-10} (1 + 106 \exp(-0.75/kT)) \text{ m},$$

$$C_B^{\text{tot}} = 1.52 \times 10^{27}/T - 3.3 \times 10^{23} \text{ m}^{-3}. \quad (27)$$

In table 1, the attenuated diffusion coefficients calculated from eqs. (18), (24) and (25) are shown along with data from Baker [21]. The numbers in the final column of table 1 relate to the numbers of gas bubbles nucleated per fission fragment and the relationship used to calculate this reflects the bubble size distribution in eq. (21). So eq. (20) must be modified to give

$$C_B^{\text{tot}} = \frac{1.52\alpha}{\pi l_f (\bar{R} + Z_0)^2}. \quad (28)$$

Baker [21] reports that occasionally as many as 100 bubbles may be counted in the wake of a fission fragment, so the figure of 24 ± 2 reported here is more consistent with experiment than the temperature-dependent yield of between 5 and 10 obtained when the simpler resolution rate (with $Z_0 = 0$) originally proposed by Turnbull [7] is used.

5. Inter-granular porosity and irradiated-induced resolution

5.1. Geometric considerations

Because of the difference between the grain-boundary energy and the free surface energy in UO_2 , the bubbles resident on grain boundaries are non-spherical in shape. Where two free surfaces meet a grain boundary, the angle between them is 2θ where the angle is controlled by the relative magnitudes of the grain boundary and free surface energies γ_{gb} and γ_{fs} respectively,

$$\theta = \arccos(\gamma_{gb}/2\gamma_{fs}). \quad (29)$$

The accepted value of θ for UO_2 is 50° [23]. The bubbles on the grain boundaries (ideally faces of a tetrakaidecahedron) are lenticular bubbles (Appendix 2) of approximately circular projection (fig. 23a). The volume of these bubbles is

$$V_{\text{gf}} = \frac{4}{3}\pi r_f^3 f_f(\theta), \quad (30)$$

$$\text{where } f_f(\theta) = 1 - \frac{3}{2} \cos \theta + \frac{1}{2} \cos^3 \theta.$$

In eq. (30), r_f is the radius of curvature of the capillary surface of the bubble and $f_f(\theta)$ relates the volume of the lens to that of the complete sphere.

The pressure inside the bubble must balance the capillary forces restraining the bubble in addition to any external mechanical forces operating. Thus, assuming the ideal gas laws, we may calculate the number of gas atoms required for mechanical stability:

$$N = PV/kT = \frac{4\pi r_f^3}{3kT} f_f(\theta) \left\{ \frac{2\gamma}{r_f} + P_{\text{ext}} \right\}, \quad (31)$$

where $\gamma = \gamma_{fs}$, the free surface energy.

The projected radius of each bubble is $r_f \sin \theta$, so if grain-face porosity saturation occurs when the fractional coverage of the grain boundaries is f_b , the "smeared" density of gas atoms over the whole grain boundary at saturation is

$$N_f^{\max} = \frac{4r_f f_f(\theta)}{3kT \sin^2 \theta} f_b \left\{ \frac{2\gamma}{r_f} + P_{\text{ext}} \right\} \text{ atoms/m}^2. \quad (32)$$

It is commonly observed that the swelling on the grain faces saturates at a value of $f_b \approx 0.25$ with a projected bubble radius r_f of typically $\sim 0.5 \mu\text{m}$ [24].

5.2. Approach to saturation-limitation by irradiation induced resolution

It is assumed that no gas release occurs from a poly-granular aggregate of UO_2 until the porosity described in section 5.1 has been established and this requires the accumulation of N_f^{\max} (eq. (32)) gas atoms per m^2 of grain boundary. Manley [9] has demonstrated that the establishment of this porosity may be delayed, particularly at lower temperatures, by the occurrence of an irradiation-induced resolution process. Although the mechanism is expected to be similar to that invoked in section 4 for the destruction of intragranular porosity, its ferocity is likely to be tamed by the large size of the grain-face bubbles. The resolution event is therefore more likely to be a "whittling away" process than the wholesale destruction of the bubbles envisaged for intragranular porosity.

Speight [3] proposed that these re-dissolved atoms

are knocked a distance δ into the grain from the grain boundary, whence they may proceed to diffuse again. The probability of such an event happening per atom per second is the resolution probability, b_r . After some time a dynamic equilibrium process will be established wherein the diffusive flux arriving at the boundaries (from two adjacent grains) exactly balances the resolution flux back into the grains. We write the concentration at δ , the resolution depth, as C^δ and hence the diffusive flux (from one grain) is DC^δ/δ . The number of atoms per unit area of grain boundary is N_f and the resolution flux is $N_f b_r/2$ into each grain. Therefore, equating these fluxes, we obtain

$$C^\delta = b_r \delta N_f / 2D. \quad (33)$$

Eq. (33) may be used to define the time for grain-face saturation to occur, (Hargreaves & Collins [1]), by demanding that the intragranular concentration produced by a gas generation rate β achieves a value just capable of surmounting the resolution barrier (eq. (32)) set up by the resolution of the grain-boundary bubble population. In this way, Hargreaves & Collins [1] define an incubation time

$$t_{\text{inc}} = b_r \delta N_f^{\max} / 2D\beta. \quad (34)$$

Speight's [3] proposals, however, enable us to be a little more precise in determining the incubation time. Eq. (33) assumes a quasi-equilibrium between boundary and resolution layer and does not provide for any release mechanism to enable the intergranular porosity to fill in the first place. One might then expect eq. (34) to be only really accurate for cases where release was very low, say, at low temperatures.

Speight [3] suggests that the Booth flux, eq. (3), is reduced by the build up of this resolution barrier. The attenuation is provided by linear interpolation of the form

$$\frac{dN_f}{dt} = 2 \times \text{Booth flux} \times \left\{ \frac{C^0 - C^\delta}{C^0} \right\}. \quad (35)$$

The factor 2 allows for release into the boundary from two adjacent grains, C^0 is the intragranular concentration and C^δ the resolution layer concentration, eq. (33).

The Booth flux from one grain is the arrival rate per unit area of grain boundary per second and may be calculated from eq. (3), that is

$$\begin{aligned} \text{Booth flux} &= \frac{1}{4\pi a^2} \frac{d}{dt} \left\{ \frac{4}{3}\pi a^3 \beta t f_c \right\} \\ &= 2\beta \left[\left(\frac{Dt}{\pi} \right)^{1/2} - \frac{Dt}{a} \right]. \end{aligned} \quad (36)$$

For simplicity we assume $C^0 = \beta t$, which presupposes

that the gas release will be small and therefore allows us to neglect the second term in eq. (36). Eq. (35) then becomes

$$\frac{dN}{dt} = 4\beta \left(\frac{Dt}{\pi} \right)^{1/2} \left\{ 1 - \frac{b_v \delta N}{2D\beta t} \right\}. \quad (37)$$

Before proceeding with the solution to eq. (37), it is worthwhile considering what effect intragranular porosity will have on the grain-boundary resolution processes. It is clear that the bulk behaviour of gas release from the grain must reflect the dynamic exchange system between matrix and intragranular bubbles existing in the interior of the grain, which leads to the effective diffusion coefficient D' in eq. (18). What is not certain is the flux between the resolution layer (at δ) and the boundary. The bubbles described in section 4 and measured by Baker [21] have radii of not much more than $\sim 10^{-9}$ m and densities $\sim 10^{23}$ m⁻³, thus the mean inter-bubble distance will be $\sim 1-2 \times 10^{-8}$ m. The resolution layer is expected to be of this order [25] so the probability of the grain boundary resolution effect reflecting the effective diffusion coefficient would appear to be remote. However, the concentration of gas in solution, C^0 , will be reduced by the same factor as the diffusion coefficient and hence C^0 in eq. (35) must be

adjusted to account for the presence of intragranular porosity. We can therefore write

$$\frac{dN}{dt} = 4\beta \left(\frac{D't}{\pi} \right)^{1/2} \left\{ 1 - \frac{b_v \delta N}{2D'\beta t} \right\}. \quad (38)$$

We make the following substitutions

$$\phi = \frac{N}{N_f^{\max}}; \quad u = \frac{4b_v \delta t^{1/2}}{(D'\pi)^{1/2}}, \quad A = \frac{\beta \pi D'^2}{8(b_v \delta)^3 N_f^{\max}}$$

and eq. (38) becomes

$$\frac{d\phi}{du} = Au^2 - \phi. \quad (39)$$

This may be integrated to yield

$$\phi = A(u^2 - 2u + 2) + Be^{-u} \quad (40)$$

and B is determined from the initial conditions.

At the commencement of the irradiation, ϕ is assumed to be zero ($\therefore B = -2A$) and grain-face saturation occurs when $N = N_f^{\max}$ or ϕ equals unity. Eq. (40) can therefore be viewed as an incubation equation. Fig. 1 shows the incubation burnup as a function of temperature for various values of free-surface energy, γ , and resolution parameter, $b_v \delta$. The value of N_f^{\max} is deduced from eq. (32) and a gas generation rate, β , of 1.65×10^{18}

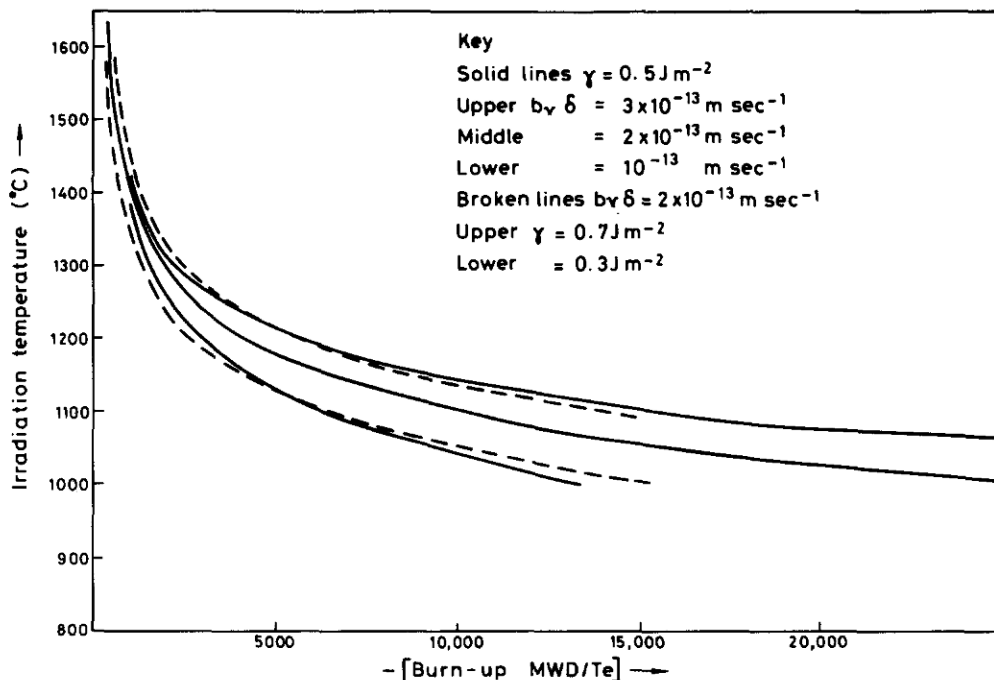


Fig. 1. Variation of incubation time in units of fuel burnup (Megawatt days/ton U) with temperature for various surface energies and resolution parameters.

$\text{m}^{-3}\text{s}^{-1}$ is assumed, which is approximately equivalent to a rating of 20 W/g in unenriched fuel. The diffusion coefficient D , from table 1 is assumed to hold. In practice D' should also be used to reflect the effect of intragranular porosity at higher temperatures.

Dowling et al. [26] have performed finite difference diffusional release calculations with an irradiation-induced resolution boundary condition and have shown that eq. (40) gives a reasonably accurate description for the kinetics of grain-face gas accumulation. The equation may be also used for approximate treatment of transient behaviour. A technique found to be useful is to assume that the intragranular concentration C^0 and the grain-face concentration ϕ_0 at the start of the irradiation period under consideration resulted from a previous anneal under identical conditions which terminated at "time" u_0 . We may then determine B in eq. (40) by assuming

$$\phi = \phi_0 \quad \text{at} \quad u = u_0,$$

where u_0 is obtained from $C^0 = \beta t_0$, β being the current generation rate. Substitution for u yields

$$u_0 = \left\{ \frac{C^0}{AC_\delta^{\max}} \right\}^{1/2}. \quad (41)$$

C_δ^{\max} is the value of the resolution layer concentration (eq. (34)) when the faces are saturated.

The transient situation has also been the subject of a finite difference simulation [27] and the comparison between the "exact" finite difference and the approxi-

mate solutions using eqs. (40) and (41) can be seen in fig. 2 for the case of downward cascading temperature history.

An important detail to note on the implementation of eq. (40) for use in fission gas release codes is that the important quantity to be stored in any computations is *not* the number of atoms per unit area of grain face but the total number of atoms on the grain faces. During any irradiation period, a certain amount of "ripening" will occur during which the overall *average* grain size will increase, yielding a decrease in the net total grain-boundary area per unit volume of fuel. Thus the concentration of fission-gas atoms per unit area of grain boundary may show an increase even though no extra atoms have diffused there.

This process is to be distinguished from the grain sweeping effect described by Hargreaves & Collins [1] and subjected to a critical reexamination by Jeffries & Tucker [28] who conclude that in most circumstances the diffusion and resolution effects predominate in grain boundary gas accumulation.

5.3. Post-incubation release

The Booth equations, eqs. (2) and (5), were derived specifically for the cases of current generation release and post-irradiation annealing release from spherical grains with perfectly absorbing boundaries. The presence of closed lenticular grain boundary porosity changes the absorption nature of the boundary in that a

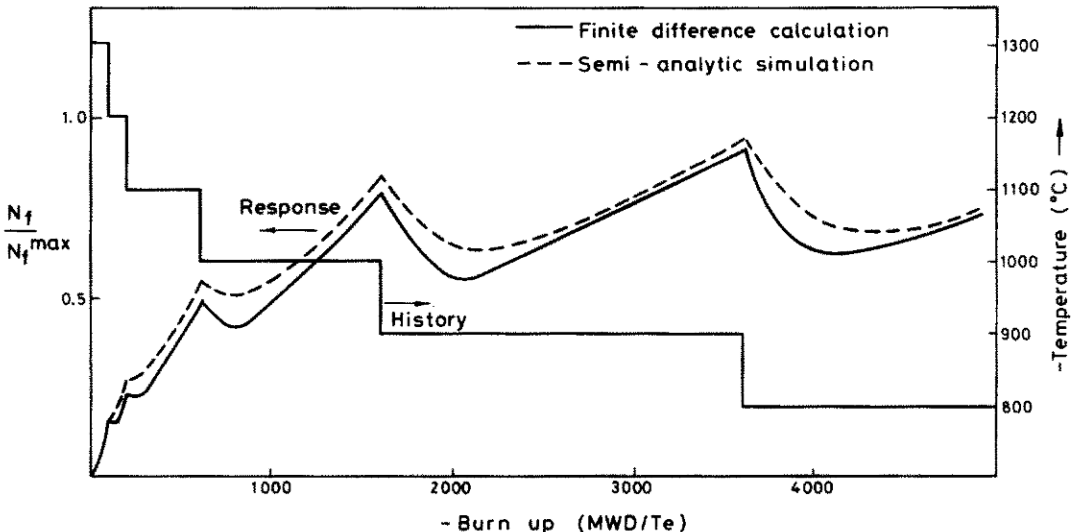


Fig. 2. Response of Finite Difference Program compared with semi-analytic technique for accumulation of gas on closed grain-boundary porosity during downward cascading fuel temperature history.

fraction of the gas atoms arriving at these bubbles will be returned, by the resolution process, back into the grain matrix and may thus continue their diffusion. The resolution distance δ is considered to be $\sim 10^{-8}$ m [25] and is therefore very much less than the radius of the grain. For this reason the approximation made by Turnbull [4] in equating the grain boundary concentration to eq. (33) would appear to be valid.

Turnbull solves the diffusion equation (eq. (1)) subject to the grain-boundary concentration being held at a value equal to the resolution layer concentration, C_δ^{\max} , pertaining at grain-boundary saturation. In addition, the intragranular concentration is initially set at C^0 ($t = 0$) and the resulting fractional release equation thus has contributions from the current generation of fission products and, if $C^0 > C_\delta^{\max}$, from the post-irradiation annealing of the supersaturation $C^0 - C_\delta^{\max}$. Turnbull's result for the total release, Q , atoms/m³ of fuel is

$$Q = f_c \beta t + (C^0 - C_\delta^{\max}) f_A, \quad (42)$$

where f_A and f_c refer to the annealing and current releases respectively and are defined in eqs. (2)–(6).

In a previous paper, White, Dowling and Tucker [27] have shown how eq. (42) may be used to simulate the

fission-gas release from a spherical grain of UO₂ subjected to a temperature and irradiation history consisting of periods of isothermal behaviour. The transient periods between adjacent isothermal periods were step-like (instantaneous) in nature. The simulation results were compared with a more accurate finite difference representation of the resolution-controlled diffusional release process and the very favourable results are shown in fig. 3.

The strategy adopted there is summarised here. At the start of an irradiation period the quantities which are known are:

Q	the total release (atoms/m ³),
β	the current gas generation rate (atoms/m ³ s),
C^0	the intragranular gas concentration (atoms/m ³)
C_δ^{\max}	the resolution barrier, eq. (34) (atoms/m ³),
N	the gas atom concentration in grain boundary bubbles (atoms/m ²).

Thus immediately from ϕ or N we may see whether gas release is "occurring", that is, whether the grain-boundary porosity is saturated. There are three options here:

- (i) $\phi < 1$

This may result either from a down temperature

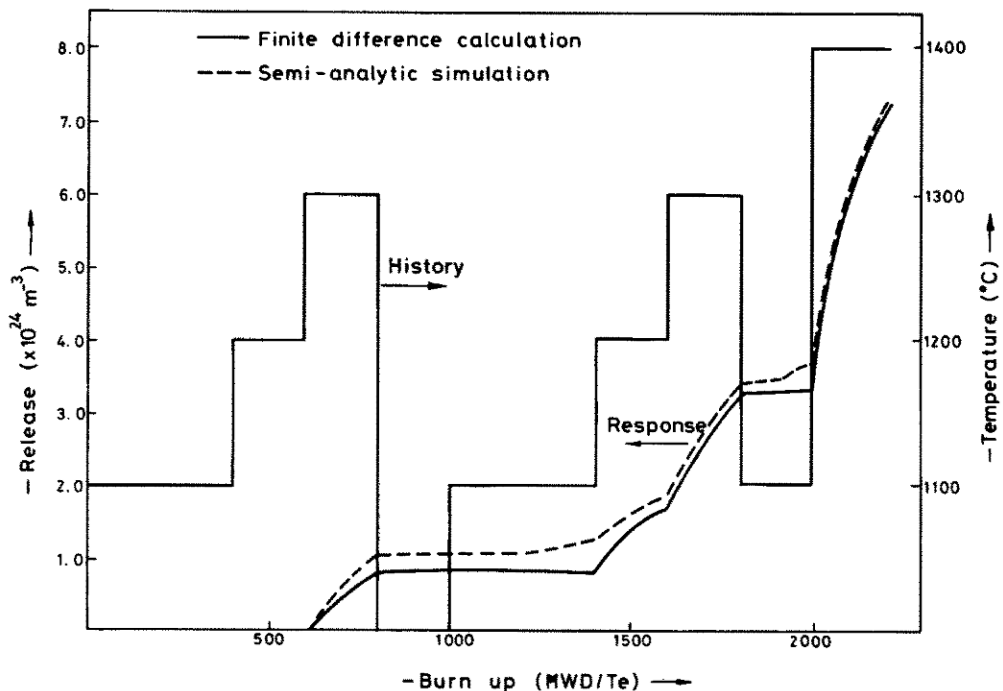


Fig. 3. Response of Finite Difference Program compared with semianalytic technique for post-incubation gas release during upward cascading cyclic fuel temperature history.

change from a situation where $\phi = 1$ as a consequence of the inverse temperature dependence of N_f^{\max} , eqs. (32)–(33), or as a natural progression toward incubation early in an irradiation. In either case, re-incubation must be established and eqs. (40) and (41) must be used.

(ii) $\phi > 1$

This will invariably result from an up-temperature change again as a consequence of the inverse temperature dependence of N_f^{\max} (eqs. (32)–(33)). This time because the bubbles are supersaturated at the higher temperature any excess gas must be “vented off” returning ϕ to unity and the “overflow” being added to Q , the total release.

(iii) $\phi = 1$

This occurs as a result of either a small temperature increase from a near-incubation situation or from a continuation of an isothermal irradiation.

Inevitably situations (ii) and (iii) will eventually be reached and the gas release must be computed. The approach adopted by White et al. [27] is to assume that the current period is a “snapshot” of a much longer hypothetical isothermal irradiation and that the effective commencement time of the “snapshot” is t . Since the only fate of stable gas atoms is release (Q) or granular retention \tilde{C}^0 , we may extrapolate back to the commencement of the hypothetical period ($t = 0$) to estimate C^0 . Hence

$$C^0 = \tilde{C}^0 - \beta t + Q. \quad (43)$$

For most situations (ii) and (iii), t may be estimated from eqs. (42) and (43). In case (i), where the grain boundaries require resaturation and $Q = 0$, a different approach may be required.

For any given value of \tilde{C}^0 it may be demonstrated (by differentiation of eq. (42)) that the maximum release obtainable, Q_{\max} , occurs when $C^0 = C_\delta^{\max}$, that is, when the release occurs from a “cold start” situation with no contribution from the post-irradiation annealing of previously generated fission gases. If the current release Q is greater than Q_{\max} , then solutions of eqs. (42) and (43) yield values of C^0 at $t = 0$ which are less than C_δ^{\max} and are thus physically unrealistic. We assume therefore that $C^0 = C_\delta^{\max}$ and that $Q = Q^{\max}$ in these situations. The value of Q^{\max} must be found from eqs. (42) and (43) and must necessarily be less than Q otherwise the previous strategy may be adopted. In relating the release to a “cold start” situation, eqs. (42) and (43) become condensed to

$$\tilde{C}^0 - C_\delta^{\max} = (1 - f_c)\beta t. \quad (44)$$

The resulting gas release predicted by these strategies is entirely independent of time step length and is a conse-

quence of the extrapolation back to $t = 0$ at the commencement of each period.

The problems encountered by Wood & Matthews [29] are effectively bypassed by this technique since the “smearing out” of the intragranular gas concentration to C^0 is performed only once per isothermal period and all subsequent subdivisions of the irradiation period refer back to that event ($t = 0$) rather than repeat the smearing out at the start of each new sub-period. The alternative strategy proposed by Matthews & Wood [30] to circumvent the difficulties encountered must also be considered redundant in the light of the success of the techniques described here, particularly since the “finite element” approach advocated does not at present handle the effects of irradiation-induced resolution.

6. The release of unstable fission products

6.1. Transient release

The standard Booth [31] treatment for the release of radiative fission products assumes a spherical UO_2 grain shape and radioactive-diffusion equilibrium such that the concentration of active species assumes a uniform steady-state profile. The relevant diffusion equation is

$$\frac{\partial c}{\partial t} = D_u \nabla^2 c + \beta_u - \lambda c, \quad (45)$$

where eq. (45) differs from eq. (1) only in the incorporation of the loss by radioactive decay. λ is the decay constant of the species in question. The Booth treatment sets $\partial c / \partial t = 0$ and for all intents and purposes this is satisfactory. On the rare occasions where the isothermal time periods are less than a few half-lives (the half-life is $0.693/\lambda$), it may be necessary to include the time-dependent transient behaviour. To facilitate the treatment of transient effects we solve eq. (45) from $t = 0$ with an initial uniform concentration C^0 of intragranular radioactive gas.

In spherical co-ordinates we obtain [32]

$$\left. \begin{aligned} c &= \frac{\beta_u}{\lambda} + \frac{U e^{-\lambda t}}{r}, \\ \text{where } U &= \frac{2}{a} \sum_{n=1}^{\infty} \exp(-X - \lambda)t \sin\left(\frac{n\pi r}{a}\right) \\ &\times \left[\int_0^a C^0 \sin\left(\frac{n\pi r'}{a}\right) r' dr' + (-1)^n \frac{\beta_u a^2}{n\pi \lambda} \right. \\ &\left. - (-1)^n \frac{n\pi \beta_u D_u}{\lambda X} (1 - \exp(Xt)) \right], \text{ with } \\ X &= n^2 \pi^2 D_u / a^2 + \lambda. \end{aligned} \right\} \quad (46)$$

The "instantaneous" release rate may be calculated from Fick's Law as

$$\tilde{R}_u = -4\pi a^2 D_u \frac{\partial c}{\partial r} \Big|_{r=a}$$

and from eq. (46) we obtain

$$\begin{aligned} \tilde{R}_u = & \frac{6D}{a^2} \left\{ \beta_u \sum_{n=1}^{\infty} \frac{1 - \exp(-Xt)}{X} \right. \\ & \left. + C^0 \sum_{n=1}^{\infty} \exp(-Xt) \right\}. \end{aligned} \quad (47)$$

For long times ($(\pi^2 D/2 + \lambda)t > 5$) the exponential terms may be neglected and the release rate reduces to a sum which sums to the steady-state Booth release:

$$\bar{R}_u = \frac{3\beta_u}{\mu} \left\{ \coth \mu - \frac{1}{\mu} \right\}, \quad \text{with } \mu = a(\lambda/D_u)^{1/2}. \quad (48)$$

In the short time limit, $D_u t/a^2 < \pi^{-2}$, the standard approximations may be made to the sums in eq. (47) [11] and we may evaluate the concentration of surviving (i.e. non-decayed) unstable release Q as

$$Q = e^{-\lambda t} \int_0^t \tilde{R}_u e^{\lambda t'} dt', \quad (49)$$

which yields

$$\begin{aligned} Q = & \frac{3\beta_u}{\mu\lambda} \left\{ \operatorname{erf} \sqrt{\lambda t} - \frac{1}{\mu} (1 - \exp(-\lambda t)) \right\} \\ & + \left\{ 6\sqrt{\frac{\omega}{\pi}} - 3\omega \right\} \left\{ C^0 - \frac{\beta_u}{\lambda} \right\} e^{-\lambda t}, \end{aligned} \quad (50)$$

with $\omega = D_u t/a^2$ as before. The release of unstable fission products during a temperature cycling and transient irradiation may be calculated using eq. (50) if a similar strategy is adopted to that used for the treatment of stable gas release (section 5).

In order to assess the accuracy of the algorithmic technique a finite difference simulation has also been performed [33].

As in the case of stable gas atoms the irradiation period in question is viewed as a "snapshot" continuation of an as yet unspecified isothermal irradiation with one extra constraint—radioactive decay. The intragranular concentration \tilde{C}^0 at the start of the period is related to the initial concentration, C^0 , by assuming a release rate \tilde{R} to have existed according to eq. (47) since $t = 0$.

Hence

$$\frac{dc}{dt} = \beta_u - \tilde{R}_u - \lambda c, \quad (51)$$

which has a solution at time t of

$$\tilde{C}^0 = \frac{\beta_u}{\lambda} (1 - \exp(-\lambda t)) - Q + C^0 \exp(-\lambda t), \quad (52)$$

where Q is given by eq. (50). Therefore, as before, the effective irradiation time may be calculated from eqs. (50) and (52).

Only one complication occurs in this analysis, since we have neglected irradiation-induced resolution; this is when the value of Q exceeds Q_{\max} , the maximum predicted by eq. (50) when $C^0 = 0$.

The value of Q at equilibrium, that is, when the supersaturation has annealed out, is given by

$$Q^{\text{equ}} = \frac{3\beta_u}{\mu\lambda} \left\{ \coth \mu - \frac{1}{\mu} \right\}, \quad (53)$$

and it may be shown that eq. (50) possesses solutions for all Q , t and \tilde{C}^0 when

$$C^0 + Q^{\text{equ}} > \beta_u/\lambda. \quad (54)$$

In fig. 4, $Q\lambda/\beta$ is plotted against λt as a function of $\tilde{C}^0\lambda/\beta$ for $\mu = 10$. For this value of μ , $Q^{\text{equ}}\lambda/\beta \approx 0.27$ (eq. (53)) and it can be seen that the maximum disappears for values of $\tilde{C}^0\lambda/\beta_u > 1 - 0.27$, i.e. 0.73, to be replaced by a monotonic climb. Therefore suitable solutions for all Q , \tilde{C}^0 and t are available in the region given by eq. (54).

In the event of the inequality in eq. (54) being reversed, we must solve eqs. (50) and (52) for t with C^0 set to zero. The release during the time period under consideration is then calculated from eq. (50) and the discarded atoms (since $Q > Q_{\max}$) allowed to evolve independently for the duration of the period. The comparison between the predictions of eqs. (50) and (52) with the finite difference treatment are shown in fig. 5.

6.2. Effect of irradiation-induced resolution

6.2a. From intragranular porosity

The effects here are likely to be similar to those calculated for stable gas atoms (section 4.2). We assume as before that the concentration c in solution in the grain may be lost by absorption at gas bubbles and enhanced by the demolition of these bubbles by passing fission fragments. Hence the concentration of gas in the grain c can be described by a marriage of eqs. (14) and (45), namely,

$$\frac{\partial c}{\partial t} = D\nabla^2 c + \beta_u + b'm - gc - \lambda c, \quad (55)$$

and the concentration in bubbles m by

$$\frac{dm}{dt} = gc - b'm - \lambda m. \quad (56)$$

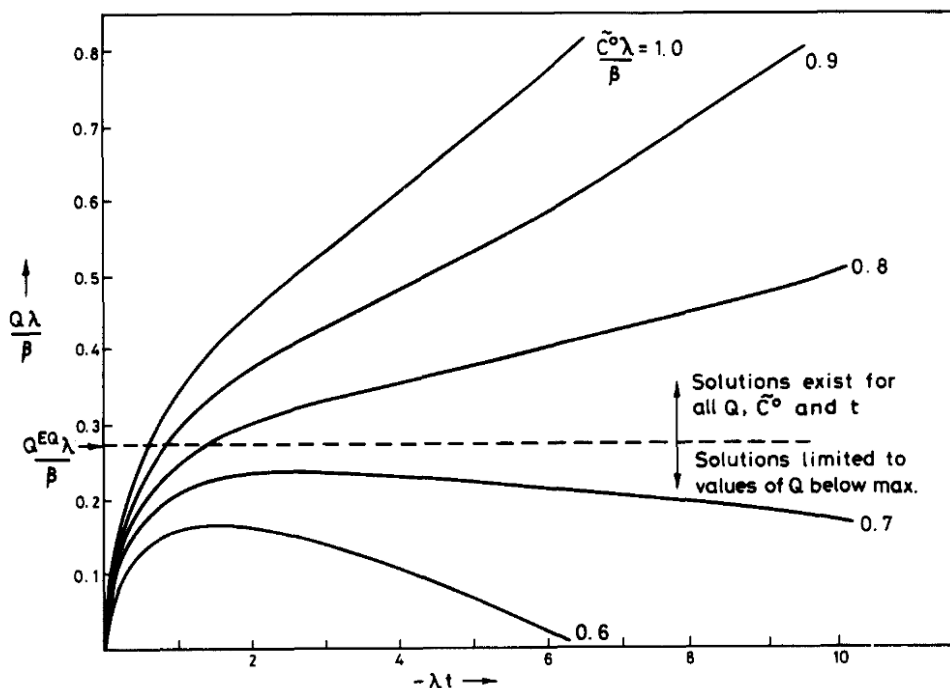


Fig. 4. Surviving unstable gas release as a function of time and initial supersaturation showing that universal solutions for Q , \tilde{C}^0 and t_0 are only available in regions above maximum.

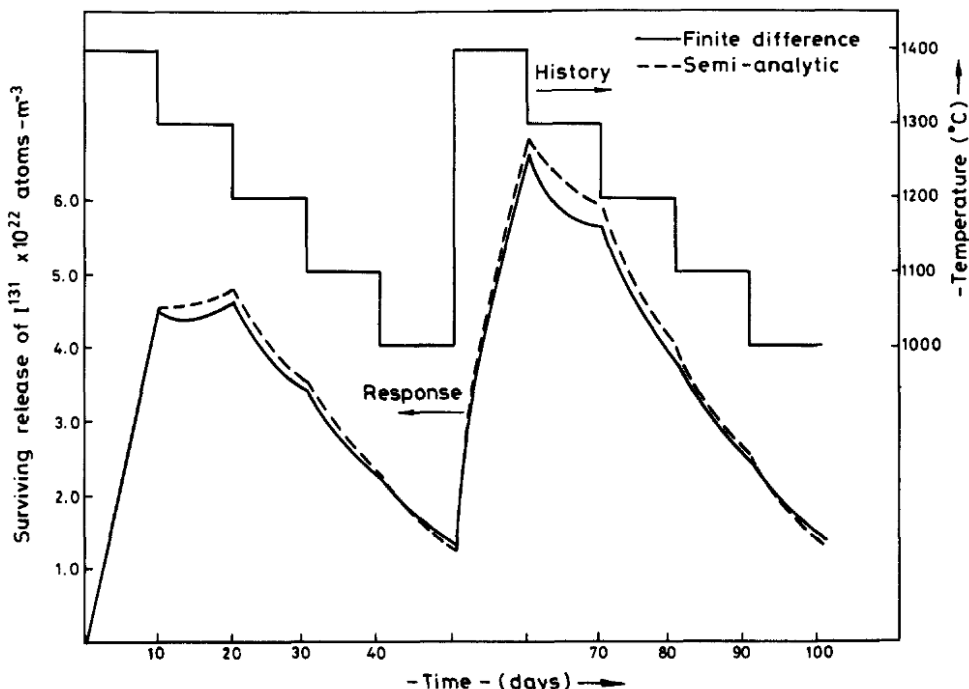


Fig. 5. Response of Finite Difference Program compared with semi-analytic solution of I^{131} (8 day half-life) for downward cascading cyclic fuel temperature history.

Adding eqs. (55) and (56), we obtain for the total gas-atom concentration $\psi = c + m$

$$\frac{\partial \psi}{\partial t} = D \nabla^2 c + \beta_u - \lambda \psi. \quad (57)$$

We assume steady state and in the case of unstable atoms this will be more readily achieved because of the radioactive decay process. Thus, substituting from eq. (56) with $dm/dt = 0$, we obtain

$$\frac{\partial \psi}{\partial t} = D \left\{ \frac{b' + \lambda}{b' + \lambda + g} \right\} \nabla^2 \psi + \beta_u - \lambda \psi, \quad (58)$$

which, as in the case of stable atoms, suggests that the standard treatments, eqs. (46)–(50), may be used with an effective diffusion coefficient defined as

$$D' = \left\{ \frac{b' + \lambda}{b' + \lambda + g} \right\} D. \quad (59)$$

6.2b. Effect of resolution from grain boundary porosity

The treatment offered by Speight [3] and repeated here (eq. (36)) for stable gas atom resolution may be modified for small releases ($\mu \gg 1$ in eq. (53)) of unstable atoms. Writing $C^0 = \beta/\lambda$ and $C^\delta = b_\nu \delta N / 2D_u$ and approximating the Booth flux, eq. (53), to the first term we have

$$\frac{dN}{dt} = \frac{2a}{3} \frac{3\beta_u}{a} \left(\frac{D_u}{\lambda} \right)^{1/2} \left\{ 1 - \frac{b_\nu \delta N \lambda}{2D_u \beta_u} \right\} - \lambda N, \quad (60)$$

where the final term accounts for decay within bubbles. The solution is

$$N = \frac{2\beta_u}{\lambda} \left(\frac{D_u}{\lambda} \right)^{1/2} \langle 1 - \exp(-\lambda \kappa t) \rangle / \kappa, \quad (61)$$

where $\kappa = 1 + b_\nu \delta / (D_u \lambda)^{1/2}$. This suggests that under steady-state conditions the concentration of atoms on the grain boundary will stabilise (assuming no venting) at a value of

$$N^{\max} = 2\beta_u (D_u / \lambda)^{1/2} / \kappa \text{ atoms/cm}^2 \quad (62)$$

or in terms of volumetric concentrations

$$Q^{\max} = \frac{3N^{\max}}{2a} = \frac{3\beta_u}{a\lambda} \left(\frac{D_u}{\lambda} \right)^{1/2} / \kappa. \quad (63)$$

It is tempting, in view of eqs. (53) and (63), to assume that the overall effect of resolution from grain-boundary bubbles is to reduce the surviving quantity of gas in these bubbles by the factor, κ . In most instances κ is likely to be very close to unity and hence the effect is probably insignificant. However, in view of the simplicity of the corrections it may be worthwhile to include the effect for completeness.

6.3. Effect of unstable atom delay at grain-face porosity

In the event of the grain-face porosity not being fully established by sufficient accumulation of stable gas atoms, unstable atoms are likely to remain trapped for an indefinite time and to decay whilst trapped, thus precluding any unstable release. After grain-face saturation, however, any excess arrival of stable atoms to the porosity must be released to the grain-edge tunnels and hence to the fuel exterior in order that the number of atoms on the face does not exceed N_f^{\max} (eqs. (32) and (33)). The average delay time t_{gf} at the grain face may be calculated from the arrival rate of stable gas atoms \dot{R}_f ($\text{m}^{-2} \text{s}$), that is,

$$t_{gf} = N_f^{\max} / \dot{R}_f. \quad (64)$$

There are clearly a number of ways of evaluating \dot{R}_f ; for example if the time period in question has a duration of Δt then we could use eq. (42) and average Q in such a way that

$$\dot{R}_f = \frac{2a}{3\Delta t} \langle Q(t + \Delta t) - Q(t) \rangle; \quad (65)$$

or we could take the instantaneous value of the derivative of Q at the midpoint of the period

$$\dot{R}_f = \frac{2a}{3} \frac{dQ}{dt} (t + \Delta t/2); \quad (66)$$

or derive the average of the derivative over Δt

$$\dot{R}_f = \frac{2a}{3\Delta t} \int_t^{t+\Delta t} \frac{dQ}{dt} dt, \quad (67)$$

which is equivalent to eq. (65).

In the event of release commencing mid-period, eqs. (65)–(67) are likely to differ; for ease of computation we prefer eq. (65) but the results from all three expressions are, on average, over many cycles, likely to differ by only trivial amounts.

7. Development of grain-edge and grain-corner porosity

7.1. The toroid model for edge porosity

The development of the gas release model for release to grain boundaries was considerably simplified by the assumption of quasi-spherical grains of UO_2 . For the treatment of grain-edge and grain-corner swelling, a more realistic grain shape must be used. The grains of UO_2 approximate in shape to a truncated octahedron or tetrakaidecahedron (TKD). The TKD has fourteen faces, six of which are square and eight hexagonal. When packed together an array of TKDs can fill all available

space in a solid and thus represents an ideal basic building block. The meeting point of each grain face is shared by two grains, of each grain edge by three grains and each grain corner by four grains. Hence, on average, each grain has seven faces, twelve edges and six corners.

Tucker [34] has further rationalised the TKD structure by assuming that the grain is composed of fourteen identical circular faces created by the compaction of fourteen right circular cones, each subtending a solid angle of $4\pi/14$ at the vertex. The cone dimensions are arranged in such a way that the volume occupied by this solid is equivalent to a TKD which is in turn equivalent to a sphere of radius a . The grain edge porosity is represented in this model by a tube threading around the circumference of the grain face; hence the name, "toroid" model. Using the geometrical properties of such an elementary building block, Tucker [34] established relationship between the volumetric swelling and surface area of coverage of triangulated grain edge porosity. For tunnels of radius of curvature r_t and semi-dihedral angle $\theta = 50^\circ$ (the most likely contender for UO_2 [23]) we have the fraction of the grain boundary area occupied by tunnels, $\Delta S/S$, given by

$$\frac{\Delta S}{S} = 1.29 \left(\frac{r_t}{a} \right) - 0.6041 \left(\frac{r_t}{a} \right)^2 \quad (68)$$

and for the fractional grain edge swelling, $\Delta V/V$, the equation

$$\frac{\Delta V}{V} = 0.5104 \left(\frac{r_t}{a} \right)^2 - 0.1613 \left(\frac{r_t}{a} \right)^3. \quad (69)$$

The equivalence between the grain-edge length (TKD) and the spherical grain model results from equation of volumes and hence

$$8\sqrt{2} l^3 = \frac{4}{3}\pi a^3, \quad \text{or} \quad l = (\pi/6\sqrt{2})^{1/3} a \quad (70)$$

and this equivalence in volume requires that the grain face radius in the toroid model, in the absence of swelling, is

$$r_{gt}^0 = 0.5557 a_0, \quad (71)$$

where a_0 is the grain radius (spherical) in the absence of swelling. The values of a and r_{gt} are modified by the presence of grain-edge swelling as follows:

$$a = a_0 (1 - \Delta V/V)^{-1/3}, \quad \text{and} \\ r_{gt} = r_{gt}^0 (1 - \Delta V/V)^{-1/3}. \quad (72)$$

In each of the sphere/TKD/toroid models the dimensions have been chosen such a way that the volumes are equivalent. It is of course impossible to arrange for

the surface areas also to be equivalent and there is in fact an increase in grain-boundary area from $12.566 a^2$ (4π) for the sphere to $13.052 a^2$ (TKD) and to $13.582 a^2$ for the toroid. There is also a less significant discrepancy in the total length of grain edge between the TKD and the toroid model.

7.2. Kinetic development of edge porosity

The lenticular grain-face bubbles described in section 5.1 will be distributed uniformly over the available grain boundary area. As a result of the near TKD-type shape, some will inevitably be close to grain edges and there will be a tendency for these to overspill [35] onto the edges where they will assume the equilibrium shape for such a situation. Clemm & Fisher [36] show that such bubbles are formed from the intersection of three spherical caps to create a triangulated (in section) cigar-shaped (in length) zepellin-type bubble (fig. 6). It is assumed that the two principal radii of curvature of such a bubble will be identical, although this does not of course follow from the Tucker and Turnbull [37] analysis of the effect of the grain-boundary energy on equilibrium bubble shapes. Clemm & Fisher [36] give the relationship between the volume of such a bubble (equal principal radii) and a sphere of the same radius, and for the particular case of $\theta = 50$, this has a value of $f_e(\theta) = 0.0517$ (see appendix 2). Finite difference calculations for the collapse of triangulated tunnels (White & Tucker [33]) suggest that the bubbles resulting from the Tucker-Turnbull [37] pressure equation could have volumes up to twice as large as those predicted from the equal principal radii assumption. Until this discrepancy is resolved, however, we will continue to utilize the Clemm & Fisher [36] results.

Calculations by Turnbull & Tucker [38] suggest that, below 1700°C at least, these bubbles will receive sufficient vacancies to enable them to grow as equilibrium gas bubbles limited by the arrival rate of stable gas atoms to the grain edges. Continued inflation will inevitably lead to the situation in fig. 6 in which a string of bubbles are just touching. Following the interlinkage of adjacent bubbles surface diffusion will tend to drive material away from regions of high to regions of low net curvature hence smoothing the tunnel profile. Unless the tunnel network constitutes more than $\sim 6\%$ volume swelling, a stable catenoidal network is not viable [33,37,39] and surface-diffusion-driven tunnel collapse will again occur, resulting in a string of larger bubbles, fewer in number and wider spaced than before. The reconnection time for bubbles clearly depends on their size, spacing and gas collection rate and the edge coales-

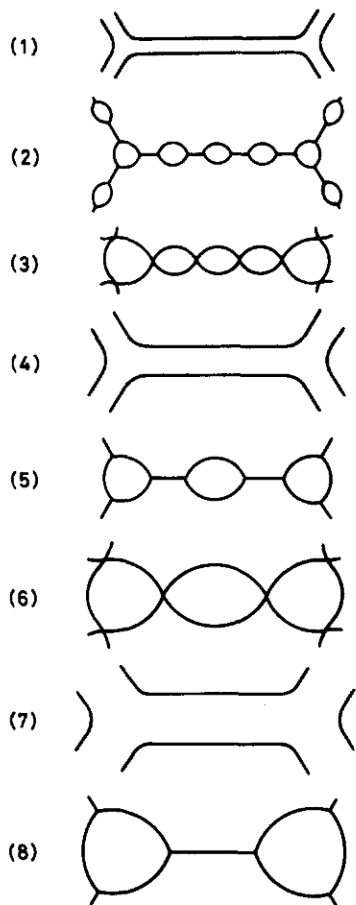


Fig. 6. Showing repeated interlinking of grain-edge bubbles and subsequent tunnel collapse leading to progressive growth of tunnel network. Note final collapse in tunnel centre.

cence-collapse sequence will continue until the resulting reformed tunnel is of such a size that it is energetically favourable for collapse to occur at a point midway along the grain edge. Beyond this point the porosity when closed remains confined to the grain corners.

Finite difference calculations for the collapse of triangulated tunnels [33] more or less substantiate the earlier findings of Tucker and White [10,40,41]. The pinch-off time of a tunnel of radius of curvature r_t varies as the fourth power of the radius, that is,

$$t_0 = a_1 \left\{ \frac{kT}{D_s \gamma \Omega^{4/3}} \right\} r_t^4, \quad (73)$$

where D_s is the surface diffusion coefficient, γ the free surface energy, and Ω is the atomic volume.

In the case of $\theta = 90^\circ$ tunnels, a_1 was of the order of

unity, being ~ 1.3 for a tunnel meeting an external surface at right angles and ~ 5 for a tunnel meeting the tetrahedrally symmetric grain corner. The distance of travel required for the surface to collapse in a triangulated tunnel is $r(1 - 2 \cos \theta / \sqrt{3})$ and this, principally, results in a much lower value of a_1 . Preliminary calculations suggest a_1 to be between 0.04 and 0.4 depending on the degree of perturbation created by the grain face or corner on the initial profile.

When a fully developed string of bubbles has been created by tunnel collapse it is found that they are spaced by an amount $2a_2 r_t$, where r_t is the initial tunnel radius. The $\theta = 90^\circ$ case yielded $a_2 = 4.19$ and from this Tucker & White [10] estimated the $\theta = 50^\circ$ case to have $a_2 = 2.07$. More detailed calculations [42] fix this parameter as 2.2, in a sense vindicating the earlier analysis.

These calculations of pinch-off time, t_0 , and bubble spacing enable us to develop a swelling model for the early stage of grain-edge swelling. Coalescence of the newly created string of bubbles occurs in a time t_c and this clearly depends on the arrival rate of stable gas atoms to the bubbles. We leave this particular calculation till later and assume here that the arrival rate \dot{R}_e atoms per metre of grain edge per second is known. At coalescence each bubble has an overall length of $2a_2 r_t$, where r_t is the initial tunnel radius of curvature prior to collapse. The volume of the bubble at this stage is (Appendix 2)

$$V_b = \frac{4}{3} \pi r_b^3 (t_0) f_e(\theta), \quad (74)$$

where

$$r_b(t_0) = \frac{a_2 r_t}{(\sin^2 \theta - \cos^2 \theta / 3)^{1/2}}$$

and as in section 5 we may calculate the number of gas atoms N_e^{\max} required to stabilise such a bubble against surface and external stress, P_{ext} , from the ideal gas law $PV = NkT$ as

$$N_e^{\max} = \frac{V_b}{kT} \left\{ \frac{2\gamma}{r_b} + P_{ext} \right\}. \quad (75)$$

Assuming that grain-boundary diffusion is sufficiently rapid to ensure that all atoms arriving on the edges will find their way to grain edge bubbles, the number of atoms arriving at each bubble per second is $2a_2 r_t \dot{R}_e$, which yields

$$t_c = N_e^{\max} / 2a_2 r_t \dot{R}_e \quad (76)$$

and for $\theta = 50^\circ$

$$t_c = 0.11452 \frac{\pi}{kT} \frac{(a_2 r_t)^2}{\dot{R}_e} \left\{ \frac{1.3403\gamma}{a_2 r_t} + P_{ext} \right\}. \quad (77)$$

The smoothing by surface diffusion ensures that after a cycle time of $t_0 + t_c$ we have returned to a triangulated cylindrical tunnel geometry, but with a new radius, say from $r_t(0) \rightarrow r_t(t_0 + t_c)$. The evaluation of $r_t(t_0 + t_c)$ may be computed as follows:

(i) A tunnel of radius $r_t(0)$ and length $2a_2 r_t(0)$ collapses into one bubble of radius $r_b(t_0)$ at time t_0 and, assuming no loss of material volume,

$$\frac{4}{3}\pi f_e(\theta) r_b^3(t_0) = 2a_2 r_t(0) \pi r_t^2(\theta) f_t(\theta), \quad (78)$$

where

$$f_t(\theta) = \frac{3}{\pi} \left\{ \theta - \pi/6 - 2 \cos \theta \sin(\theta - \pi/6)/\sqrt{3} \right\},$$

relates the cross-sectional area of a triangulated tunnel to that of a circular tunnel of the same radius of curvature [37] (see Appendix 2). For $\theta = 50^\circ$, $f_t(\theta) = 0.0909$.

(ii) After a length of time $t_0 + t_c$ these bubbles have just reconnected and at this point

$$r_b(t_0 + t_c) = \frac{a_2 r_t(0)}{\left(\sin^2 \theta - \frac{1}{3} \cos^2 \theta \right)^{1/2}}. \quad (79)$$

(iii) The final smoothing process turns this bubble to a cylinder of radius $r_t(t_0 + t_c)$ and

$$\frac{4}{3}\pi r_b^3(t_0 + t_c) f_e(\theta) = 2a_2 r_t(0) \pi r_t^2(t_0 + t_c) f_t(\theta). \quad (80)$$

This ultimately gives

$$r_t(t_0 + t_c) = r_t(0) \left\{ \frac{a_2}{\left(\sin^2 \theta - \frac{1}{3} \cos^2 \theta \right)^{1/2}} \times \left\{ \frac{2f_e(\theta)}{3f_t(\theta) \left(\sin^2 \theta - \frac{1}{3} \cos^2 \theta \right)^{1/2}} \right\}^{1/2} \right\}, \quad (81)$$

and for $\theta = 50^\circ$

$$r_t(t_0 + t_c) = 1.12 a_2 r_t(0) \quad (82)$$

which describes the tunnel radius increase per cycle.

By assuming that the radius increases linearly with time through the cycle we may write the instantaneous rate of increase of tunnel radius r_t as

$$\frac{dr_t}{dt} = \frac{r_t(0)}{t_0 + t_c} (1.12 a_2 - 1) \quad (83)$$

and because the average period length Δt is likely to be much less than $t_0 + t_c$, we can in most cases assume

$$r_t(t + \Delta t) = r_t(t) + \frac{dr_t}{dt} \Delta t. \quad (84)$$

In the event of Δt being greater than $t_0 + t_c$ it may be safer to apply eq. (82) as many times as necessary and

use eq. (84) for the residual time step. Finally, the grain-edge swelling, $\Delta V/V$, may be calculated from the toroid relationship, eq. (69).

This mode of swelling continues until the pinch-off occurs in the middle of the grain edge and this condition is met when $r_t > l/2a_2$. From then on, the swelling is confined to the corners, but first we must evaluate \dot{R}_e , the arrival rate of atoms per unit length of grain edge.

As with the case of \dot{R}_f in section 6.3, there are a variety of ways of evaluating \dot{R}_e .

If the grain-face bubbles are not saturated then the only atoms arriving at the tunnels are those resulting from the pre-incubation flux described by eq. (38). We call this \dot{N}_f and the capture area for tunnels is $S \times \Delta S/S$, where $\Delta S/S$ is given by eq. (68). S may be $14\pi r_{gf}^2$, $4\pi a^2$ or $(14 + 8\sqrt{2})l^2$ depending on whether the toroid, sphere or TKD model is assumed. Likewise, the total grain-edge length is either $14\pi r_{gf}$ or $36l$, depending on toroid or TKD geometry. Using the toroid model in the pre-incubation period, we may write the arrival rate of stable atoms per unit length of grain edge as

$$\dot{R}_e = \left. \begin{aligned} &\frac{1}{2} \frac{14\pi r_{gf}^2}{14\pi r_{gf}} \frac{\Delta S}{S} \dot{N}_f \\ &= 0.834 a \frac{\Delta S}{S} \dot{N}_f. \end{aligned} \right\} \quad (85)$$

Alternatively, we could assume spherical grains each with $36l$ (TKD) grain-edge length and in this case

$$\dot{R}_e = 0.73 a \frac{\Delta S}{S} \dot{N}_f. \quad (86)$$

In the post-incubation period all atoms arriving at the grain faces at rate \dot{R}_f (as given by eqs. (65)–(67)) will eventually reach the grain edges and hence, reducing this to atoms per unit length of grain edge and incorporating the pre-incubation flux (calculated from eq. (85) or (86)), we obtain

$$\dot{R}_e = \left\{ \begin{aligned} &0.73 \\ &0.834 \end{aligned} \right\} a \left\{ \frac{\Delta S}{S} \dot{N}_f + \dot{R}_f \right\}. \quad (87)$$

The evaluation of \dot{N}_f is clearly subject to the same ambiguities as that for \dot{R}_f and probably the most sensible assumption is to write

$$\dot{N}_f = \{ N_f(t + \Delta t) - N_f(t) \} / \Delta t, \quad (88)$$

where the values of N are derived from eq. (38).

7.3. Kinetic development of grain-corner porosity

The bubbles which form in the grain corners after the collapse of tunnels with radius $r_t > l/2a_2$ have been

described by Clemm & Fisher [36]. Their appearance is that of a tetrahedron constructed of four spherical segments of radius r_c , the four vertices extending along the grain edges (fig. 7). The volume of such a bubble is

$$V_c = \frac{4\pi}{3} r_c^3 f_c(\theta), \quad (89)$$

where for the $\theta = 50^\circ$ case $f_c(50) = 0.0209$, from Appendix 2.

We again assume that the supply of vacancies to the bubbles is sufficient to constrain bubble growth to gas-atom supply limitation. At the point of interlinkage the distance from the corner centre to the bubble vertex d_c is equal to half the grain-edge length. For a $\theta = 50^\circ$ corner bubble, $d_c = 0.4078 r_c$ (Appendix 2), and hence $r_c^{\max} = 1.226/0.88a = 0.88a$, and again assuming the ideal gas laws we may equate the number of gas atoms in a corner bubble to the surface and external stresses, P_{ext} :

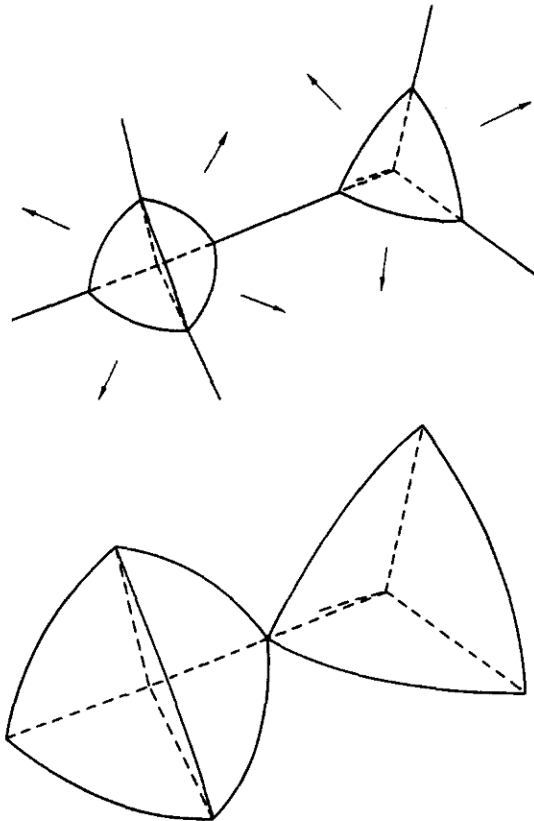


Fig. 7. Development of grain-corner swelling following curtailment of grain-edge mode in fig. 6.

with some manipulation we obtain

$$N_c^{\max} = 0.0194 \frac{\pi a^3}{kT} \left(\frac{2.27\gamma}{a} + P_{\text{ext}} \right). \quad (90)$$

Assuming the arrival rate of gas atoms to a corner bubble is \dot{R}_c (atoms/s) we may write

$$t_c = N_c^{\max}/\dot{R}_c. \quad (91)$$

After the collapse of a large ($r_t > l/2a_2$) grain-edge tunnel, we have shown in Appendix 1 that the average time delay before grain corner reconnection is $\frac{3}{4}t_0 + \frac{7}{4}t_c$. In order to evaluate the effective swelling rate we require the initial grain corner bubble radius $r_c(0)$. This may be evaluated in one or two ways (at least):

(i) The bubble resulted from the collapse of four edge tunnels, each of radius $l/2a_2$ and each of which will have partitioned half of their volume to one corner, therefore

$$\frac{4\pi}{3} r_c^3(0) f_c(\theta) = 4 \frac{l}{2} \pi \left(\frac{l}{2a_2} \right)^2 f_T(\theta). \quad (92)$$

Assuming $a_2 = 2.2$ (section 7.2) and $\theta = 50^\circ$, we have

$$r_c(0) = 0.4956a. \quad (93)$$

(ii) Assuming the toroid model [34] and $a_2 = 2.2$, the initial edge-swelling at point of collapse with $r_t = l/2a_2 = 0.1632a$ is $\Delta V/V = 1.29\%$ (eq. (69)). A TKD type grain has six corners per grain and hence this swelling is partitioned over six corner bubbles. Thus

$$\frac{\Delta V}{V} = 6 \times \frac{4}{3}\pi r_c^3(0) f_c(\theta) / \frac{4}{3}\pi a^3, \quad (94)$$

from which, for $\Delta V/V = 1.29\%$, we obtain

$$r_c(0) = 0.4655a \quad (95)$$

and the difference is insignificant.

The growth in radius of the bubble over a time period $3/4 t_0 + 7/4 t_c$ is thus from $0.4956a$ (or $0.4655a$) to $0.88a$ and, assuming a linear rate of growth, we may write

$$\frac{dr_c}{dt} = \frac{1.54a}{3t_0 + 7t_c}. \quad (96)$$

Complete interlinkage of the tunnel network will occur in this model when $r_c = 0.88a$ which, using eq. (94), results in a swelling of 8.7%. Previous calculations based on the equilibrium curvature of a catenoidal system of tunnels suggests that stability is attained for swelling between 5 and 6.5% for $\theta = 50^\circ$ [37, 39, 42].

In view of this it is perhaps reasonable to terminate this mode of swelling when $\Delta V/V$ exceeds $\sim 6\%$.

The time that a complete corner bubble remains closed is t_c and this, from eq. (91), requires an estima-

tion of the arrival rate of gas atoms, \dot{R}_c . The fractional grain area occupied by bubbles is no longer given by the toroid formula (eq. (68)), so we must once again resort to Clemm & Fisher [36]. The surface area of a corner bubble (with $\theta = 50^\circ$) as a fraction of the equivalent sphere surface area is $f_{AC}(\theta) = 0.0913$ (Appendix 2). Thus, since a TKD grain has 24 corners each shared between four other grains,

$$\left. \begin{aligned} \frac{\Delta S}{S} &= 6f_{AC}(\theta) \left(\frac{r_c}{a} \right)^2 = 0.541 \left(\frac{r_c}{a} \right)^2 \\ \text{and from eq. (94)} \\ \frac{\Delta V}{V} &= 6f_c(\theta) \left(\frac{r_c}{a} \right)^3 = 0.128 \left(\frac{r_c}{a} \right)^3. \end{aligned} \right\} \quad (97)$$

Extending the reasoning leading to eq. (87), we may write the arrival rate of atoms to each corner bubble as

$$\begin{aligned} \dot{R}_c &= 4\pi r_c^2 f_{AC}(\theta) \left\{ \frac{\Delta S}{S} \dot{N}_f + \dot{R}_f \right\} \\ &= 1.133 r_c^2 \left\{ \frac{\Delta S}{S} \dot{N}_f + \dot{R}_f \right\}. \end{aligned} \quad (98)$$

In this case $\Delta S/S$ is given by eq. (97). The other parameters \dot{N}_f and \dot{R}_f are defined in eqs. (65)–(67) and (88). The only remaining uncertain parameter is the pinch-off time t_0 and it seems most reasonable to relate the corner bubble volume to its equivalent grain-edge tunnel radius in order to apply eq. (73). Thus, since each corner bubble is equivalent to four $l/2$ length tunnels, we obtain for $\theta = 50^\circ$

$$r_t (\text{equivalent}) = 0.466 (r_c^3/a)^{1/2}. \quad (99)$$

Alternatively the equivalent swelling (eqs. (69) and (97)) may be used.

The fourth power dependence of eq. (73) does not appear to hold much above $r_t = l/2a_2$ [33] and it may be more realistic to assume a law of the form

$$t_0 = a_1 \left(\frac{kT}{D_s \gamma \Omega^{4/3}} \right) \left(\frac{l}{2a_2} \right)^2 r_t^2 \quad \text{for } \frac{l}{2a_2} < r_t < l/a_2, \quad (100)$$

and

$$t_0 = \frac{a_1}{4} \left(\frac{kT}{D_s \gamma \Omega^{4/3}} \right) r_t^4 \quad \text{for } \frac{l}{a_4} < r_t. \quad (101)$$

These latter two expressions represent the finite difference data much more realistically.

7.4. Swelling above stable tunnel interlinkage

At $\Delta V/V \sim 6\%$ the tunnels and corners are assumed to remain open indefinitely, so neither of the modes of

swelling described previously can operate. Since swellings in excess of 6% are observed experimentally, we choose to use the values of swelling rate already incorporated into the MINIPAT [1] fuel modelling code. These values are outlined in Appendix 3.

8. The poly-granular aggregate model for unstable gas release

8.1. Model concept

Prior to irradiation, the single UO_2 grains may be considered to be tightly sintered together with only a limited presence of porosity, none of it produced by irradiation and most of it unintentionally left after imperfect manufacturing techniques. It is assumed that the geometrical shape of this fuel, and the initial imperfections present, define an effective surface area for release such that the surface-to-volume ratio may be crudely imagined as a large sphere of radius A . This radius will obviously depend on the manufacturing route, initial density and controlled porosity introduced into the fuel as well as the basic UO_2 grain size, a .

The concept of release from the large grain involves three separate processes:

(i) Diffusion fields will be established within the large sphere and a contribution to release direct from the geometric surface will occur.

(ii) The release from small true grains to intergranular bubbles and to grain-edge tunnels will, by virtue of the decay process, give rise to an effective unstable gas atom generation rate which differs from the irradiation-induced generation of gas atoms.

(iii) The "effective" gas atom production will be free to "diffuse" to the surface of the large sphere "A" by a "percolation diffusion" process. This percolation diffusion operates by means of the opening and closing of the grain edge and corner porosity during the development of the swelling process.

8.2. Direct loss from the outer geometric free surface of "A"

We assume here that the appropriate diffusion coefficient for the unstable species, D' , and the decay constant, λ , have been corrected for the presence of intra (true) granular porosity as in eq. (59). The diffusion equation for release to the free surface (equation (45)) is solved in spherical symmetry for the large grain of radius A and true gas generation rate β . The release rate

\tilde{R}_i atoms ($m^{-3}s^{-1}$) follows from eq. (48) that is,

$$\tilde{R}_i = \frac{3\beta_u}{\mu_i} \left\{ \coth \mu_i - \frac{1}{\mu_i} \right\}, \quad (102)$$

with $\mu_i = A\sqrt{\lambda/D'}$.

8.3. The effective generation rate β'

As in section 8.2, D' is the diffusion coefficient modified by trapping at intergranular gas bubbles. The rate of arrival of undecayed atoms on grain boundaries divided by the intragranular production rate is eq. (48) (Booth [31]), which can be written

$$\left\{ \frac{\tilde{R}}{\beta_u} \right\}_g = \frac{3}{\mu_{ii}} \left\{ \coth \mu_{ii} - \frac{1}{\mu_{ii}} \right\}, \quad (103)$$

where $\mu_{ii} = a\sqrt{\lambda/D'}$.

In the event of steady state not being achieved, the transient calculation (section 6.1) must be used. The transient calculation deals in surviving concentrations so over a time period Δt in which the initial surviving release was $Q(0)$ and final surviving release $Q(\Delta t)$ we could assume a uniform value of R/β equal to

$$\left\{ \frac{\tilde{R}}{\beta_u} \right\}_g = \frac{\lambda}{\beta_u} \left\{ \frac{Q(\Delta t) - Q(0) \exp(-\lambda\Delta t)}{1 - \exp(-\lambda\Delta t)} \right\} \quad (104)$$

and Q is evaluated in eq. (50).

At all times, both before and after grain-face saturation, a fraction ($\Delta S/S$) of atoms reaching the grain boundaries according to eqs. (103) or (104) diffuse straight to grain-edge or corner porosity. The value of $\Delta S/S$ must of course reflect the swelling mode which is operating, eq. (68) being appropriate for grain edge and eq. (97) for grain-corner swelling. The remaining fraction, $1 - \Delta S/S$, is retained on the grain faces until these become saturated. The subsequent release to the grain edges may be calculated by assuming that each atom trapped in a lenticular bubble suffers a dwell time t_{gf} , given by eq. (64). If there are Q undecayed atoms per unit volume residing in grain-face lenticular bubbles, it follows that the change in numbers is given by

$$\frac{dQ}{dt} = \left\{ 1 - \frac{\Delta S}{S} \right\} \left\{ \frac{\tilde{R}}{\beta_u} \right\}_g \beta_u - \lambda Q - \frac{Q}{t_{gf}}, \quad (105)$$

where the third term represents the "seepage" rate of unstables from the grain-face porosity. We consider it to be slightly more realistic to represent the release of products from the grain face as a seepage mechanism rather than the "pulse" method adopted previously by Turnbull and Friskney [12]. In actuality there is very little to choose between the two approaches in terms of

the results they yield, but a continuous release representation is more in accord with the physical ideas inherent in a diffusion calculation.

Solving eq. (105), assuming that $Q = Q(0)$ at $t = 0$, and averaging the release rate Q/t_{gf} over the time period Δt , gives

$$\begin{aligned} \left\{ \frac{\tilde{R}}{\beta_u} \right\}_{eff} &= \frac{(1 - \Delta S/S)}{\lambda' t_{gf}} \left\{ \frac{\tilde{R}}{\beta_u} \right\}_g \\ &\times \{1 - (1 - \exp(-\lambda'\Delta t))/\lambda'\Delta t\} \\ &+ Q(0)\{1 - \exp(-\lambda'\Delta t)\}/\lambda'\Delta t t_{gf} \beta_u, \end{aligned} \quad (106)$$

where $\lambda' = \lambda + t_{gf}^{-1}$.

Assuming that the fraction of the grain boundary occupied by tunnels receives the unattenuated Booth release $\langle R/\beta \rangle_g$ we may write the effective production rate of unstables per unit volume, β_{eff} , of undecayed atoms in the tunnels as

$$\frac{\beta_{eff}}{\beta_u} = \left\{ \frac{\tilde{R}}{\beta_u} \right\}_g \frac{\Delta S}{S} + \left\{ \frac{\tilde{R}}{\beta_u} \right\}_{eff}. \quad (107)$$

For long-lived isotopes at low temperatures ($\sim 1000^\circ C$) it may be worthwhile to include the effects of irradiation-induced resolution from the grain-boundary lenticular porosity, in which case eq. (107) becomes

$$\frac{\beta_{eff}}{\beta_u} = \left\{ \frac{\tilde{R}}{\beta_u} \right\}_g \frac{\Delta S}{S} + \left\{ \frac{R}{\beta_u} \right\}_{eff} / \kappa \quad (108)$$

and κ is defined in eq. (61).

8.4. The effective diffusion coefficient for gas release by way of percolation through the grain-edge tunnel network

The probability, p , of finding a tunnel of internal radius of curvature r_i open at any time may be written as

$$p = t_0/(t_0 + t_c). \quad (109)$$

Here t_0 is the pinch-off time appropriate to the aspect ratio (radius/length) of the tunnel [eqs. (73), (100) and (101)], and t_c is likewise the time required to re-open a grain-edge bubble [eqs. (76), (77), (85) and (88)] or a grain corner bubble [eqs. (90), (91) and (98)].

When this probability is small, the gas atoms entering the grain edge pores and contributing to the effective production rate will probably have to remain trapped within a grain corner until one of the four edges leading from the corner becomes open. This event will bring the trapped atoms into contact with a greater quantity of fission gas contained within a larger volume of porosity, and by gaseous diffusion each of the origi-

nal atoms have an equal probability of being found subsequently in any part of this volume.

We have demonstrated previously that an effective diffusion coefficient may be derived which is related to the aperiodic opening and closing of the tunnel system. We taken this opportunity here of correcting a normalisation error in the original calculation, and full details are given in Appendix 1. The frequency of opening (and closing) of a grain corner ν_c may be written in terms of the time to re-open an individual grain-edge bubble or grain corner as

$$\nu_c = 5/t_c. \quad [\text{eq. (A7)}] \quad (110)$$

The mean square distance travelled by any individual gas atom during a period in which a corner is open is

$$\overline{d^2} = l^2/2(1-p)^3, \quad (111)$$

An effective diffusion coefficient D_{eff} may be defined on random walk grounds in terms of the frequency ν_c and the mean square flight distance $\overline{d^2}$ and the release of gaseous fission products from an aggregate of UO_2 grains with intermittently open grain edge porosity may be considered as a diffusion process, with D_{eff} given by *

$$D_{\text{eff}} = \frac{1}{6} \nu_c \overline{d^2} = 5l(1-p)^3/12t_c. \quad (112)$$

Assuming that radioactive equilibrium is attained in the diffusion process, we may thus write

$$D_{\text{eff}} \nabla^2 c + \beta_{\text{eff}} - \lambda c = 0 \quad (113)$$

for the PGA of radius A . Release will of course occur from the other surface of this PGA by the standard intragranular diffusion process [eq. (102), section 8.2] in addition to the gaseous diffusion along the intermittently open intergranular edge and corner porosity. Thus the gross release may be written as the sum of two terms

$$\begin{aligned} \left\{ \frac{R}{\beta_u} \right\}_{\text{total}} &= \frac{3}{\mu_i} \left\{ \coth \mu_i - \frac{1}{\mu_i} \right\} \\ &+ \frac{3}{\mu_{\text{eff}}} \left\{ \frac{\beta_{\text{eff}}}{\beta_u} \right\} \left\{ \coth \mu_{\text{eff}} - \frac{1}{\mu_{\text{eff}}} \right\}, \end{aligned} \quad (114)$$

where $\mu_{\text{eff}} = A\sqrt{\lambda/D_{\text{eff}}}$.

The first term is the direct true diffusional release from the outer surface of the fuel described in section 8.2, whilst the second describes the percolation release arising from the intermittently open porosity. Each term is of course identical in form to the original Booth calcula-

* It is arguable that the factor 6 should be 4 owing to the tetrahedral symmetry of a grain corner and the fact the movement is constrained along one of four grain edges.

tion. We have not used the transient behaviour calculation for the effective diffusion model since this calculation is only valid for $\pi^2 D t / A^2 < 1$, a condition not always met under the conditions in which the model is applied. In fact, an accurate numerical series solution of the transient model under conditions of $\pi^2 D t / A^2 > 1$ differs very little from the steady-state solutions described here.

It is also possible to employ the concept of the effective diffusion coefficient, D_{eff} , in a very different way and yet obtain results which are only negligibly different. We assume that a "seepage" model may be used to describe the release of unstables from the aggregate and that the seepage is characterised by a leakage time τ_L . It is thus possible to write for the average intra-aggregate-concentration N

$$\frac{dN}{dt} = \beta_{\text{eff}} - \lambda N - \frac{N}{\tau_L}, \quad (115)$$

the solution of which is

$$\left\{ \frac{R}{\beta} \right\} = \frac{N}{\tau_L} = \frac{1}{1 + \lambda \tau_L} \left\{ 1 - \exp \left\{ - \left(\lambda + \frac{1}{\tau_L} \right) t \right\} \right\}. \quad (116)$$

The average seepage time may be described in terms of the effective diffusion coefficient, D_{eff} , (eq. (112)), as

$$\tau_L = \bar{R}^2 / D_{\text{eff}}, \quad (117)$$

where \bar{R} is the mean distance from inside the sphere to the surface. This is given by averaging over all shells within a sphere of radius A , giving

$$\bar{R} = \int_0^A 4\pi r^2 (A-r) dr / \frac{4}{3}\pi A^3 = \frac{A}{4}. \quad (118)$$

This means that on average a gas atom must travel a mean distance of one quarter of the radius to escape from the grain, and therefore that

$$\tau_L = a^2 / 16 D_{\text{eff}}. \quad (119)$$

Using $\omega_E = D_{\text{eff}} t / A^2$, we obtain

$$\frac{R}{\beta} = \frac{1}{1 + \mu_{\text{eff}}^2 / 16} \left\{ 1 - \exp \left\{ - (\mu_{\text{eff}}^2 + 16) \omega_E \right\} \right\}, \quad (120)$$

which shows similar behaviour to eq. (114) for small values of μ_{eff} .

9. Parameter values

9.1. General

The model presented in sections 2-8 for the release of stable and unstable fission products from irradiated

UO_2 contains many physical variables and constants. Some of these, such as atomic volumes, decay constants, fission yields and gas generation rates, are reasonably well characterised and the uncertainties are quite small. Others, however, such as diffusion coefficients, surface energies and resolution parameters are not only difficult to measure but show alarming lack of consistency from experiment to experiment; it is becoming clear that factors like oxide stoichiometry and annealing environment may affect up to an order of magnitude changes in measured values. For this reason, it must be impossible to define an "correct" value for the diffusion coefficient or the surface energy. The best we can do is to use "median" or averaged values or even to use the model described here as interpretive device with which to determine new or improved values.

The single gas atom diffusion coefficient D proposed by Turnbull et al. [14] is a good case in point. The line drawn by Turnbull passes through the centre of gravity of a scatter diagram of diffusion coefficient versus inverse temperature. At any one temperature the actual measured values of D may differ from the Turnbull line by a factor of five up or down! Now this must also reflect uncertainties in other areas, for example, temperature uniformity and determination, rating uniformity and determination, grain size, etc. The same lack of consistency is found in surface energy determinations and the only firm commitment that can be made here is that the value lies in the range 0.2–1.0 J/m².

Ultimately, of course, the uncertainties may be used advantageously as "tuning" devices with which to tailor the code to suit various types of fuel, and it may be necessary for surface energies, etc., to be treated as being fuel-type dependent.

9.2. Well characterised parameters

(i) Fission gas generation rates β and decay constants λ

The generation rate of stable gas atoms (Xe , Kr) per m³ of fuel depends on the fission rate and the yield for fission. Schilling [43] has provided a formula relating the generation rate to the fuel enrichment E and the rating W_R (W/g)

$$\beta = 2.9 \times 10^{16} \left\{ 2.606 + \frac{0.6386}{1 + 375E/W_R} \right\} W_R \text{ atoms/m}^3\text{s.} \quad (121)$$

The corresponding expression for unstable atoms does not contain any corrections for enrichment (in need of revision perhaps?) and is

$$\beta_u = 2.9 \times 10^{17} W_R Y^i \text{ atoms/m}^3\text{s.} \quad (122)$$

Table 2

Isotope	Fractional yield Y^i	Decay constant λ (s ⁻¹)
I^{131}	0.0293	9.98×10^{-7}
I^{133}	0.0669	9.21×10^{-6}
Xe^{133}	0.0669	1.52×10^{-6}
Xe^{138}	0.066	8.17×10^{-4}
Kr^{88}	0.035	6.73×10^{-5}

The Y^i values are the fission yields for the isotopes of interest and the values of these and the corresponding decay constants are given in table 2. The particular values used are derived from Katcoff [44] and Crouch [45].

(ii) Atomic volumes, b , Ω

b is the Van der Waals volume and the value used is that for xenon of 8.5×10^{-29} m³/atom. The atomic volume Ω is derived from theoretically dense UO_2 fuel and is 4.1×10^{-29} m³/atom.

9.3. Less well characterised parameters

(i) Gas atom diffusion coefficient, D

The single gas atom diffusion coefficient described in section 4 is adopted as the "fixed commodity" in all calculations performed here for stable gas release. In view of the uncertainties and deviations from the Turnbull line [14] for certain isotopes it is necessary to consider that unstable atoms may move faster or slower than single stable gas atoms. For each isotope in table 2 we have therefore chosen to scale the diffusion coefficient by a fixed amount, thus,

$$D^i = \alpha^i D, \quad (123)$$

where the α^i are chosen to assist consistent experimental interpretations. In addition to this correction, account is also taken intragranular porosity for which the revised Baker [21] corrections (table 1) are used.

(ii) Surface diffusion coefficient, D_s

This is calculated from measurements of scratch decay [46] or grain-boundary grooving [47,48]. The method of analysis employs the Mullins [49,50] solutions to the surface diffusion equation and relies on an accurate estimate of γ since D_s and γ appear together as a product. The work of Hodkin and Nicholas [47,51] indicates that oxide stoichiometry has a considerable effect on the magnitude of D_s . Because of this, and the general agreement on the temperature dependence for

stoichiometric fuel, we choose to adopt the Reynolds [46] values

$$D_s \gamma = 5.6 \times 10^2 \exp(-5.15/kT) \text{ J/s.} \quad (124)$$

(iii) The free surface energy γ

This parameter is the subject of a continuing debate [47,48,52,53]. The values reported for free surface and grain-boundary energies indicate a semi-dihedral angle $\theta \approx 75^\circ$, in contrast to the value of 50° currently accepted from scanning micrographs of fractured UO₂ surfaces [23]. Since all surface energy measurements are performed on external surfaces it may indicate that contamination of the surface is an important factor in modifying free surface behaviour. Also there appears to be a strong dependence on stoichiometry. In view of these uncertainties, we have experimented with values between 0.3 and 0.7 J/m² and the results are discussed later.

(iv) The irradiation-induced resolution from grain boundaries, parameter $b_\nu \delta$

The depth of penetration of a redissolved atom δ is expected to be less than 10^{-8} m [25], and the resolution probability b_ν is unlikely to exceed or even be as large as b' , the destruction probability for small intragranular porosity (eq. (26)). For a fission rate $\sim 10^{19}$ m⁻³s⁻¹ and a bubble radius $\sim 10^{-9}$ m, b' is of the order of 2×10^{-3} s⁻¹. So if the grain boundary resolution process operated with 1% of the efficiency of the intragranular process we might expect $b_\nu = 2 \times 10^{-5}$ s⁻¹. The composite parameter $b_\nu \delta$ has been assumed to be in the region of 10^{-13} m/s [1], which suggests that the efficiency of resolution from grain boundaries is much less than from intragranular bubble destruction. One would expect the value of $b_\nu \delta$ to be dependent on fission rate and since the simplest measure of this is fuel rating (W/g) it is convenient to write

$$b_\nu \delta = (b_\nu \delta)^0 W_R / W_R^0, \quad (125)$$

where $(b_\nu \delta)^0$ is the resolution parameter at some arbitrary rating W_R^0 .

9.4. Complete experimental unknowns

In this group of parameters we have a_1 , the pinch-off proportionality factor (eq. (73)), a_2 the bubble spacing (after pinch-off) parameter and A the poly-granular aggregate radius. Note of these parameters are in any way quantified by previous experimental observations and for the first two, one must establish the approximate values from theoretical considerations. Finite dif-

ference calculations modelling the collapse of triangulated tunnels indicate that a_1 lies between 0.04 and 0.4, depending on the perturbation exerted by the existence of grain corners. Similarly, the array of bubbles left after total collapse points to a value of 2.2 for a_2 . a_2 appears to be independent of initial perturbation as one would expect since the second bubble is always created from the perturbation generated by the formation of the first bubble. It might be thought that scanning electron micrographs of grain-edge porosity would reveal the bubble spacing, but this is not the case because there is no way of knowing how much bubble growth has occurred since tunnel collapse.

The radius, A , of the poly-granular aggregate defines the level of early unstable release and hence should, if diffusion coefficients are known with any certainty, be easy to estimate. Its value will clearly depend on the presence of cracks and thus could decrease with increasing irradiation. This is not expected to be a serious problem, especially in high release pins, because after long irradiation times the tunnel network will become fully stabilised and the release from intergranular pores will be total anyway.

10. Parametric comparisons

10.1. Philosophy

An exhaustive study of the effects of changing the various parameters outlined in section 9 would perhaps serve only to confuse. For this reason, it is better to limit our attention to changes in one or two key parameters whilst maintaining the other parameters fixed at the "most likely" values. As an exercise we have chosen to examine the behaviour of the stable gas release and the release rates of I¹³¹ (8 day half-life) and Xe¹³⁸ (14 minute half-life) along with the grain-edge and corner swelling for an isothermal three hundred day anneal. The temperature considered is 1400°C and the rating is assumed to be fixed at 20 W/g, which is typical of AGR-type irradiation. The radius of the poly-granular aggregate is 2×10^{-4} m and the UO₂ grain radius is 5×10^{-6} m. The iodine diffusion coefficient is assumed to be three times larger than that of stable gas atoms and xenon atoms.

10.2. Stable gas release

This is shown in fig. 8 for values of surface energy 0.3, 0.5 and 0.7 J/m² and resolution parameter of 10^{-13} and 3×10^{-13} m/s. As one would expect, the increase in

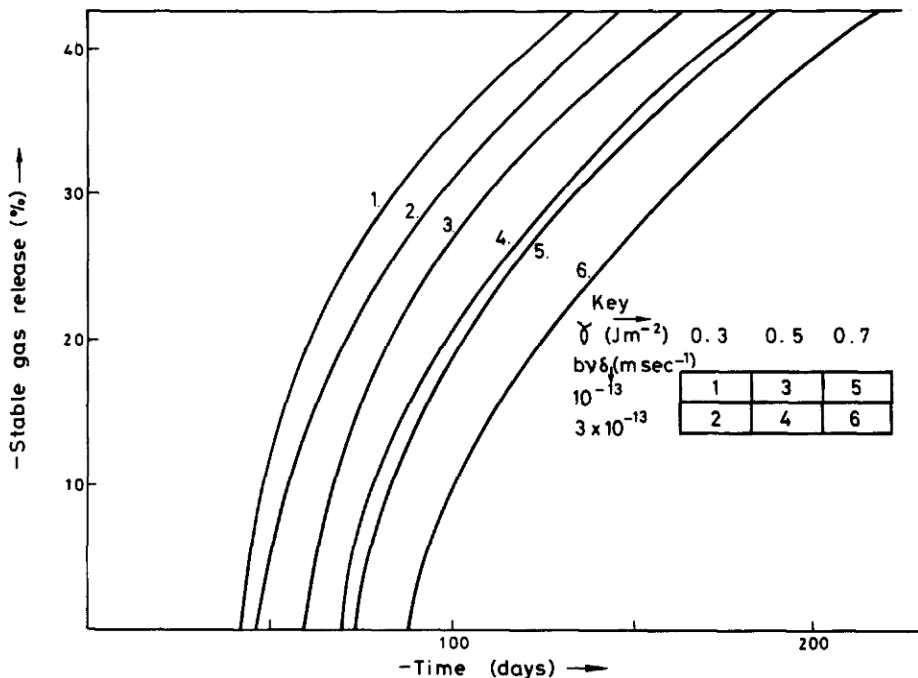


Fig. 8. Variation of stable gas release at 1400°C with surface energy γ and resolution parameter b,δ .

surface energy delays the onset of gas release through the increase in capacity of the grain faces. The increase in resolution parameter has a correspondingly larger effect at larger values of surface energy and this is simply because there are more atoms on the grain faces available for resolution. Qualitatively, the post-incubation release is very similar for all values of γ and b,δ , the overwhelming effect of changes in these parameters being on the duration of the incubation period.

10.3. Grain-edge swelling

Using values of $a_1 = 0.1$ and $a_2 = 2.5$ for the pinch-off and bubble-spacing proportionalities, the variation of $\Delta V/V$ arising from grain edge and corner swelling with the same range of γ and b,δ is shown in fig. 9. The onset of rapid swelling occurs simultaneously with the saturation of the grain faces (incubation). This is arrowed in the figure. The onset of this period is delayed, as is the stable gas release, by increasing values of surface energy and resolution parameter. Above 6%, the swelling is controlled by the semi-empirical rules in Appendix 3.

An important difference between this model and that proposed by Tucker and White [10] which comes to light here is the absence of the enhanced release of

unstables prior to grain-face saturation. The reason that this occurred in the previous approach was that a simple linear grain-edge swelling model was applied from the beginning of the irradiation thus allowing tunnel growth to occur independently of grain-face bubble growth. The present model, being more physically based, avoids this problem.

10.4. Unstable release

The release/birth rates of I^{131} and Xe^{138} are shown in figs. 10a and 10b, for the same values of γ , b,δ , a_1 and a_2 used in sections 10.2 and 10.3. The effect of surface energy on unstable release is much more dramatic here than for stable whereas the resolution parameter exerts very little control. The reasons for this are twofold, firstly through the effect on stable release and secondly through the control of grain-edge and corner-bubble dynamics. The surface energy both affects the number of atoms in these bubbles, and hence their reconnection times t_c and the pinch-off time for tunnel collapse, t_0 .

Both isotopes exhibit the plateau for short times ($t < 40$ days). This is controlled by the value of the poly-granular aggregate radius and scales inversely as A

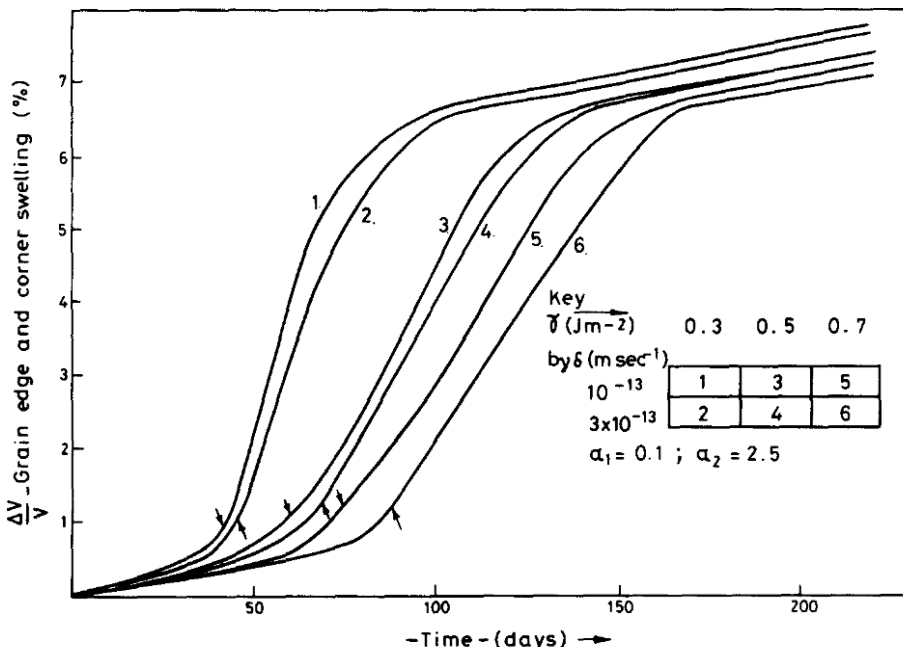


Fig. 9. Variation of grain-edge and corner swelling at 1400°C with surface energy and resolution parameter. The pinch off proportionality $\alpha_1 = 0.1$ and the bubble spacing parameter $\alpha_2 = 2.5$.

(eq. (102)). Xe^{138} having a half-life of only ~ 14 minutes, the release rate continues to rise as the swelling increases above 6%, since more and more of the grain face becomes exposed to permanently open tunnels, thus

reducing the delaying effect of grain-face porosity. Even a short delay time in grain-face bubbles affects the Xe^{138} release, whereas the iodine 131 atom with a half life of 8 days rapidly attains a stable release rate.

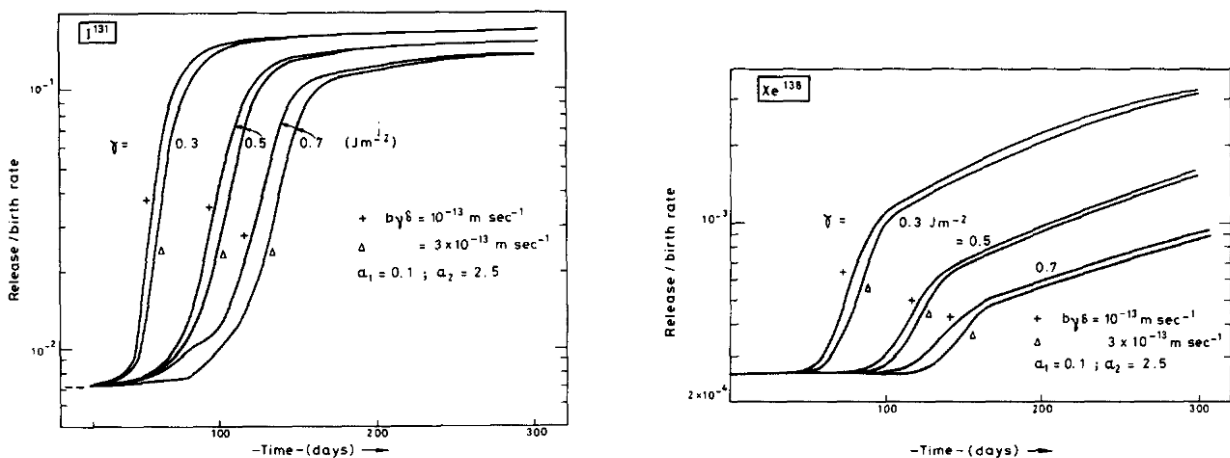


Fig. 10. Release over birthrate of (a) I^{131} and (b) Xe^{138} for same conditions as in fig. 9.

10.5. Effects of variations of a_2 , the bubble spacing parameter

For these calculations the surface energy is set at 0.5 J/m^2 and the resolution parameter $\sim 2 \times 10^{-13} \text{ m/s}$. The pinch-off proportionality a_1 is set at 0.1 and the bubble spacing parameter a_2 is varied through 1.5, 2.5 and 3.5. The effect of the grain edge and corner swelling appears to be negligible (fig. 11) until a_2 exceeds 2.5, beyond which point the onset of swelling is delayed by $\sim 20\text{--}30$ days. This effect is mirrored almost exactly in the unstable fission product release rates, figs. 12a and 12b. Physically an increase in a_2 indicates that tunnel collapse results in fewer, larger, more spaced-out bubbles. Hence the time to reconnect is increased and the swelling rate reduced. In addition to this, the swelling at which transfer from the grain edge to grain-corner swelling mode is effected is lowered.

10.6 Effects of variations of a_1 , the pinch off proportionality parameter

The values of surface energy and resolution parameter are as used in 10.4 and 10.5. The value of a_2 is fixed

at 2.5 and a_1 varied through 0.01, 0.1 and 1.0. The effect of variations in a_1 on the grain edge and corner swelling is shown in fig. 13 and a_1 clearly exerts far more control than a_2 in limiting the swelling rate. In all cases the swelling rate increases after the saturation of the grain faces and there is no apparent discontinuity at the changeover from grain edge to grain corner swelling ($\sim 1.2\%$).

The unstable release rates again reflect the sensitivity to a_1 (figs. 14a and 14b), the shorter-lived isotope Xe^{138} being more affected than the longer lived I^{131} . The behaviour of I^{131} appears to be anomalous in that the $a_1 = 0.1$ curve saturates at a lower release rate than when $a_1 = 1.0$. The reason for this must be because although the tunnels are predominantly open ($p = 0.99$ for $a_1 = 1$ at $t = 250$ days as against $p = 0.97$ for $a_1 = 0.1$) the grain edge swelling and hence fractional grain area exposed ($\Delta S/S$) is less for higher values of a_1 . Ultimately the $a_1 = 0.01$ curve will saturate at a higher plateau than either.

10.7. Summary

The main conclusions to be drawn from this section are:

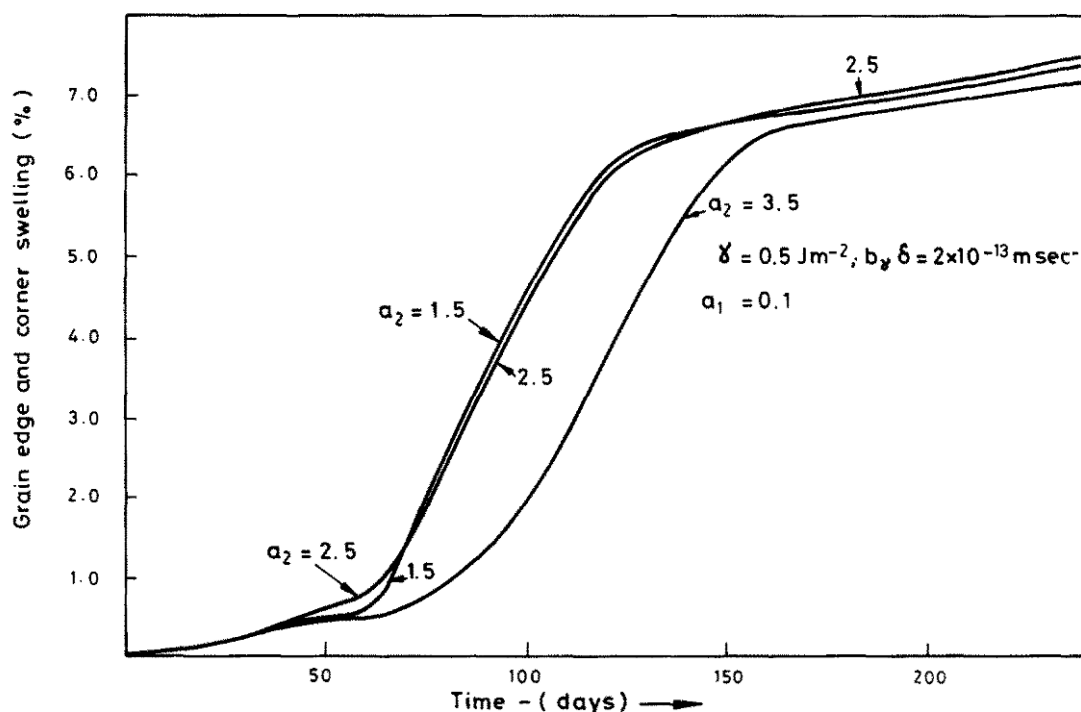


Fig. 11. Variation of grain-edge and corner-swelling at 1400°C surface energy $\gamma = 0.5 \text{ J/m}^2$, resolution parameter, $b_*\delta = 2 \times 10^{-13} \text{ m/s}$ and pinch off proportionality $a_1 = 0.1$. Note insensitivity for $a_2 < 2.5$.

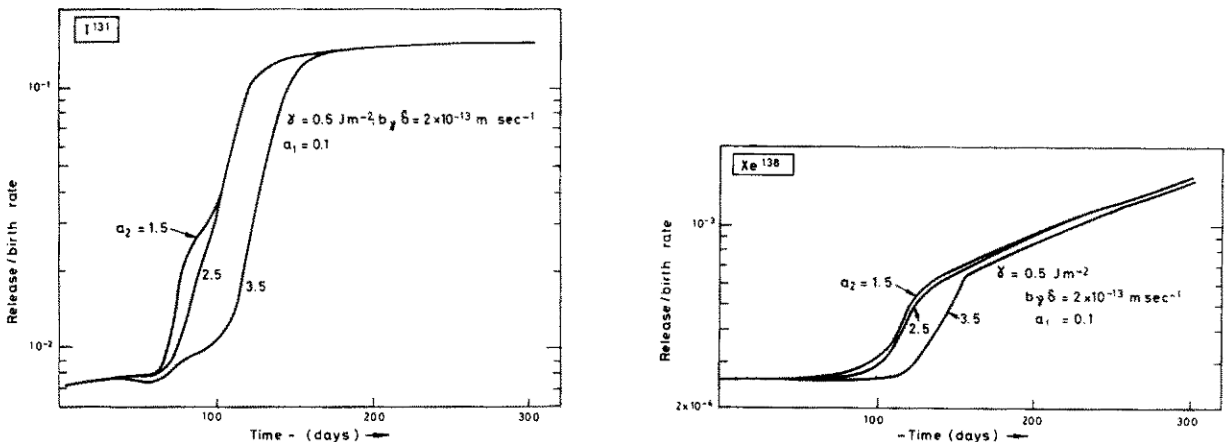


Fig. 12. Release/birthrate of (a) I^{131} and (b) Xe^{138} for conditions in fig. 11.

- (1) Increasing the surface energy γ leads to a higher capacity for gas on the grain faces and longer incubation times.
- (2) Increasing the resolution parameters $b_y \delta$ results in higher resolution rates hence longer incubation times. the effect is compounded when γ is also increased owing to the greater number of grain face atoms available for resolution.
- (3) The grain-edge swelling rate increases after incubation, the onset of which is controlled by γ and $b_y \delta$.
- (4) The onset of the unstable fission product release ramp is controlled by the surface energy and to a lesser extent by the resolution parameter.

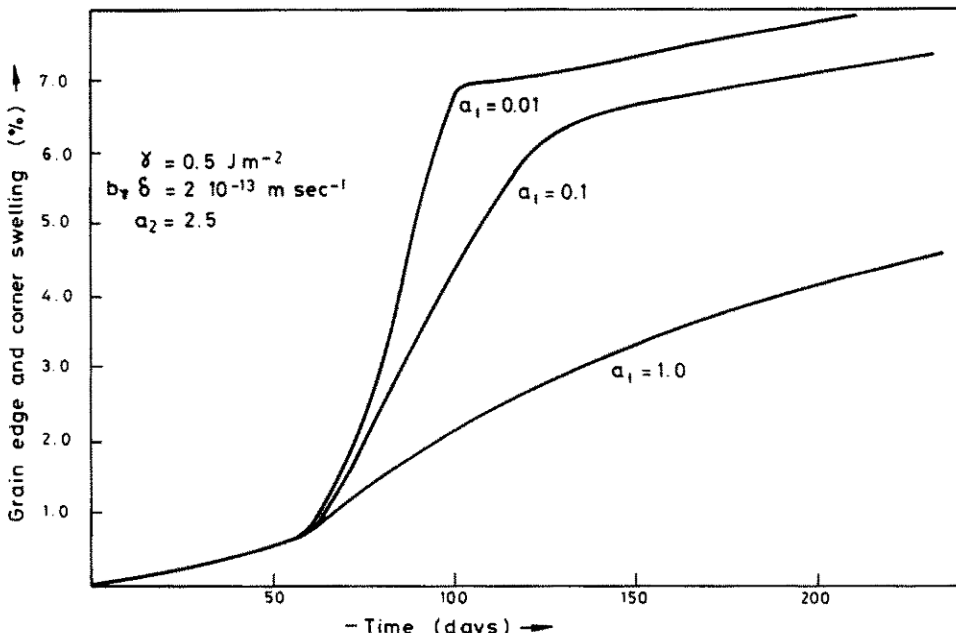


Fig. 13. Variation of grain-edge and corner swelling at 1400°C with pinch-off proportionality, a_1 . Surface energy $\gamma = 0.5 \text{ J/m}^2$, resolution parameter $b_y \delta = 2 \times 10^{-13} \text{ m/s}$ and bubble spacing $a_2 = 2.5$.

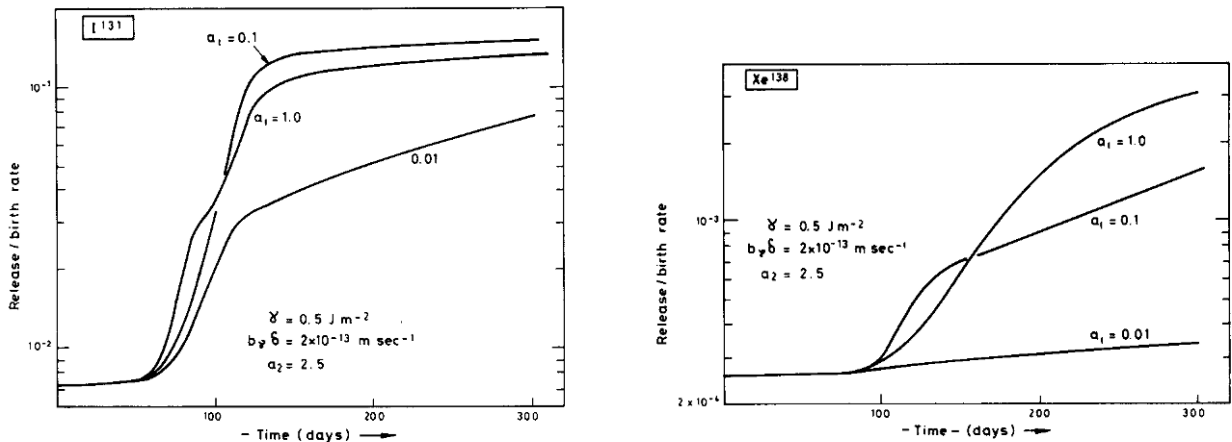


Fig. 14. Release/birthrate of (a) I¹³¹ and (b) Xe¹³⁸ for conditions in fig. 13.

- (5) Shorter-lives isotopes do not reach a plateau as rapidly as long lived ones as a consequence of the dependence on storage in grain face bubbles.
- (6) The grain-edge swelling rate is insensitive to change in the value of a_2 (the bubble spacing parameter) below 2.5.
- (7) Above $a_2 = 2.5$ increases in a_2 retard the onset of the higher swelling rate (above 1%) but does little to effect the maximum swelling rate.
- (8) Values of a_2 less than 2.5 have little effect on the unstable release rate. Above 2.5 the unstable release mirrors the delay in onset of increased swelling rate.
- (9) Increasing a_1 , the pinch-off proportionality, reduces the swelling rate dramatically.
- (10) Increasing a_1 accelerates the release of unstable fission products.
- (11) The plateau for short-time release is controlled by release from the outer surface of the poly-granular aggregate and is thus inversely proportional to this radius.
- (12) Very little unstable release, apart from that from external geometrical surfaces, occurs until the grain faces have been saturated.

11. Experimental results

11.1. The data

Turnbull and Friskney [12] have reported measurements made on release rates of several radio-isotopes from sintered spheres of 1.46%-enriched stoichiometric

UO₂. The experiment, which was nominally an isothermal irradiation, was performed in a heated rig in the DIDO reactor at UKAEA Harwell. A rating/temperature/time history has been prepared for this experiment [54] and this is shown in Appendix 4. It will be seen that each reactor "period" consists of one day at ~ 700°C, during which the electrical heaters are switched off, followed by three weeks at ~ 1400°C during which the electrical heaters are operating. A "cold finger" situated close to the samples collected volatile fission products during the irradiation period and these were removed for counting during the three or four day shutdown period.

11.2. The simulations

The values of diffusion coefficients and other key parameters have been discussed in sections 9 and 10. For the purposes of simulation of the Turnbull and Friskney data, we have assumed all the parameters apart from a_1 , a_2 , A , γ and $b_y \delta$ to have the values quoted in section 9. For the scaling of unstable atom diffusion coefficients we have found the values listed in table 3 to be suitable (eq. (123)). These values suggest that the iodine atom diffuses several times more rapidly than a stable gas atom whereas a krypton atom moves much more slowly. No great physical significance should be attributed to these numbers, however, since the Turnbull [19] diffusion coefficient, adopted for stable atoms, is only a "best fit" line through widely scattered experimental data. In addition to this, no account has been taken of precursor diffusion effects.

A value of 0.2 has been adopted for a_1 and the finite

difference result of 2.2 is used for the bubble spacing parameter, a_2 . The short-time release rates are reasonably well accounted for by choosing a poly-granular aggregate radius of 2×10^{-4} cm and any changes in this value would require power of two changes in the diffusion coefficient scaling factors used in table 3.

The only remaining parameters to exercise any control over the release rates are γ , the surface energy and $b_s\delta$, the resolution parameter. These parameters control the duration of the incubation period and hence the onset of stable gas release. Unfortunately this point was not measured experimentally and can only be inferred from the prompt rise in unstable release rates after 130–150 days. Values of γ in the region of 450 erg/cm² and $b_s\delta = 2 \times 10^{-11}$ cm/s give an incubation period of typically ~ 130 days when the power history in Appendix 4 is adopted. In view of the fact that the grain-face saturation immediately precedes the prompt increase in swelling and unstable release rate, figs. 9 and 10, the values of γ and $b_s\delta$ would appear to be constrained to values not greater than $\pm 20\%$ from those used here.

For the simulations the order of computation was as follows:

- Each isothermal period subdivided into a number of equi-length subperiods, usually 2, 5 or 10.
- Stable gas release calculated with the resolution parameter being weighted by the fraction of closed grain face porosity [55]. This closed porosity reflects conditions during the previous subperiod and hence two is the minimum number of acceptable period sub-divisions.
- Average arrival rate of gas atoms at grain faces calculated in (ii) used to evaluate bubble opening (t_c) times and tunnel pinch-off (t_0) times enabling swelling rates and effective poly-granular aggregate diffusion coefficient to be calculated.
- Release of unstable atoms evaluated.

The predicted stable gas release is independent of the number of period sub-divisions as long as at least two are used. The unstable product release, being more

Table 3

Isotopes	Diffusion coefficient scaling factor α^i (eq. (123))
I ¹³¹	3.0
I ¹³³	2.0
Xe ¹³³	2.0
Xe ¹³⁸	1.0
Kr ⁸⁸	0.2

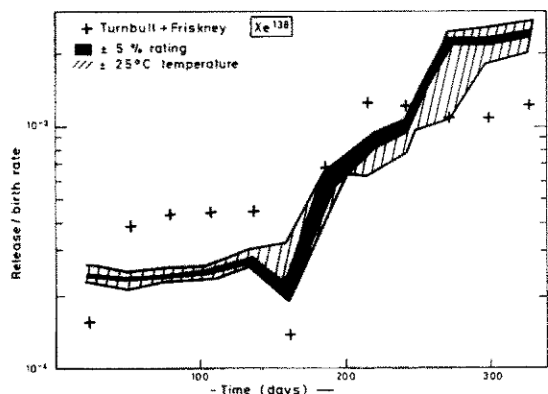


Fig. 15. Release/birthrate for Xe¹³⁸ given history in Appendix 4. Parameter details given in sections 10 and 11. Band = $\pm 5\%$ rating error, hatched $\pm 25^\circ\text{C}$ error.

dependent on the swelling rate, is more sensitive to the number of period sub-divisions but even here the discrepancy in going from 10 \rightarrow 2 sub-divisions is less than that created by a 5% uncertainty in rating or a $\pm 5^\circ\text{C}$ uncertainty in temperature. This is shown by the narrow band of predictions in figs. 15–19. The larger spread in figs. 15–19 is typical of a $\pm 25^\circ\text{C}$ temperature uncertainty and the latter figure is of the order of uncertainty quoted for the Turnbull and Friskney [12] experiment.

The overall quality of the predictions in figs. 15–19 is very good. The model appears to be capable of reproducing the transient nature of the release rates, for example in the dip in release rates between 120 and 180 days in Kr⁸⁸, Xe¹³³ and Xe¹³⁸. Of course, it may be

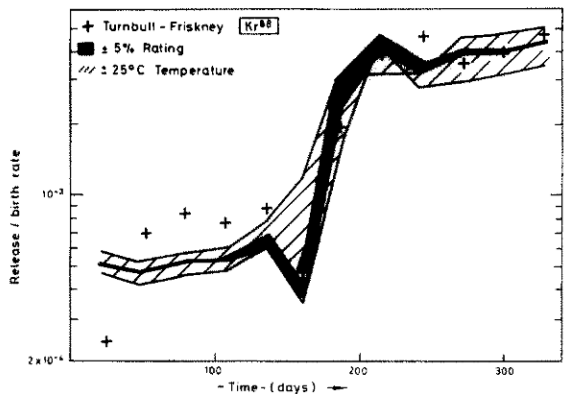


Fig. 16. Release/birthrate for Kr⁸⁸ given history in Appendix 4. Parameter details given in sections 10 and 11. Band = $\pm 5\%$ rating error, hatched $\pm 25^\circ\text{C}$ error.

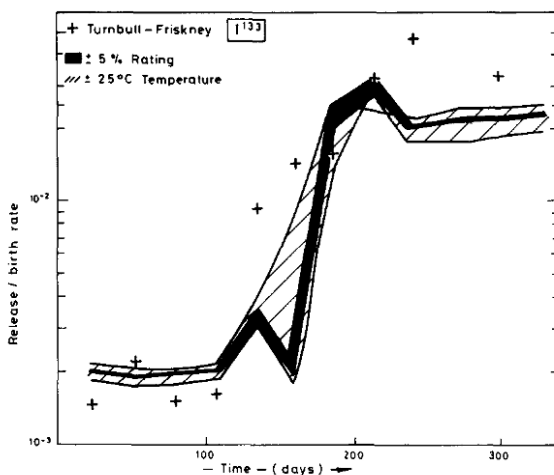


Fig. 17. Release/birthrate for I^{133} given history in Appendix 4. Parameter details given in section 10 and 11. Band = $\pm 5\%$ rating error, hatched $\pm 25^\circ C$ error.

argued that the actual experimental data contains some anomalies, this dip being present in the short lived isotopes Xe^{138} (14 mins), Kr^{88} (2.84 hrs) and the longer lived Xe^{133} (5.24 days) but absent in the intermediate I^{133} (20.8 hrs).

The model predicts this dip for all five isotopes considered except when the temperature history is in

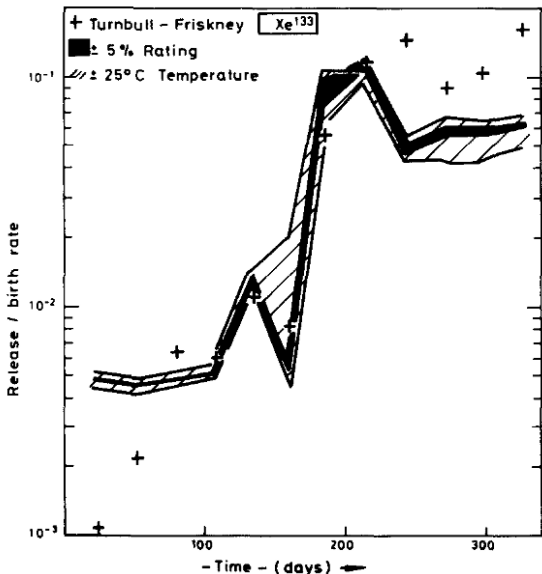


Fig. 18. Release/birthrate for Xe^{133} given history in Appendix 4. Parameter details given in section 10 and 11.

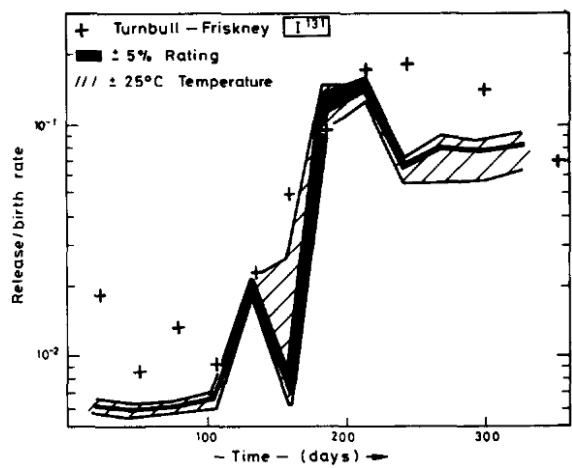


Fig. 19. Release/birthrate for I^{131} given history in Appendix 4. Parameter details given in sections 10 and 11. Band = $\pm 5\%$ rating error, hatched $\pm 25^\circ C$ error.

error by $+25^\circ C$, in which case the dip is absent and since all the isotopes were released from one sample the dip should be either present in all or none of the

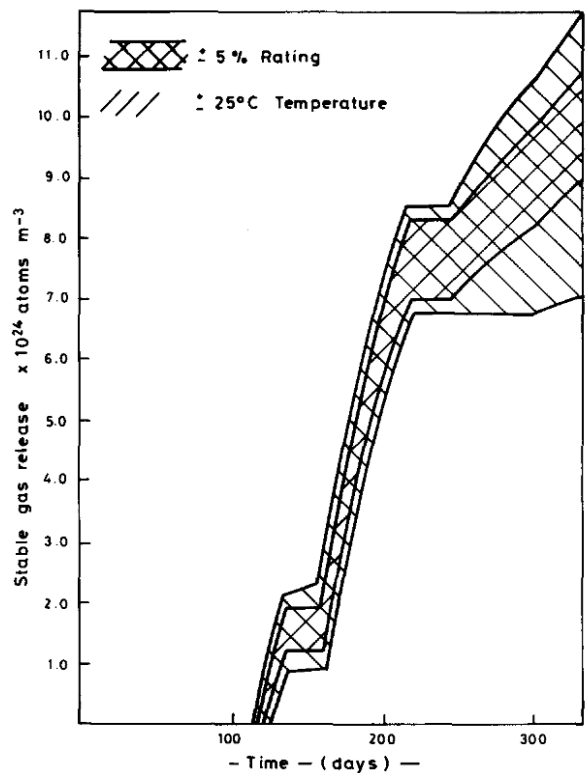


Fig. 20. Stable gas release for history in Appendix 4.

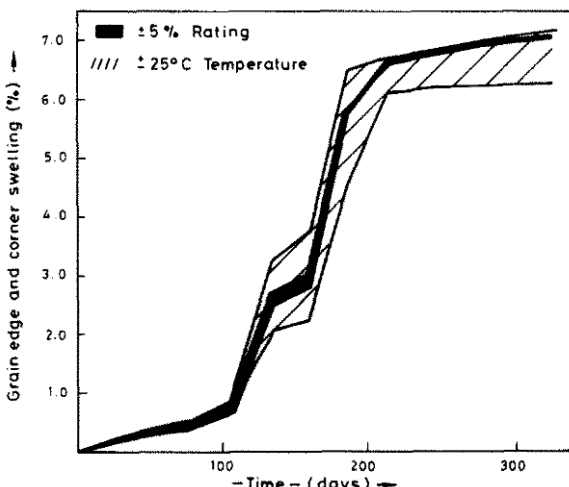


Fig. 21. Grain-edge and corner swelling in Appendix 4.

isotopes. There are two possible causes for this discrepancy. The first, error in experimental measurement, is beyond the scope of this paper. The second is that the unstable product diffusion coefficients are in error over the critical temperature region 1150–1450°C. Another indicator in favour of this conclusion is the behaviour for times greater than 200 days. At this stage the porosity is virtually fully open so the only available delaying mechanism for unstables is trapping at closed grain face porosity. Yet the release rate is underpredicted by a factor of two or three for I^{131} , I^{133} and Xe^{133} and overpredicted for Xe^{138} . The Turnbull et al. [14] diffusion coefficients were calculated from unstable release rates without consideration of a delaying mechanism at the grain faces so the discrepancy could be simply resolved by using the present model to evaluate revised diffusion coefficients.

The stable gas release is shown in fig. 20 but no conclusions can be drawn from the absolute values because no experimental details are available for comparison. The same comments obviously apply to the grain edge and corner swelling in fig. 21.

12. Conclusions

A theoretical model has been developed which describes the release kinetics of fission gases and unstable volatile fission products from irradiated UO_2 fuel.

The release of stable fission gases is assumed to be delayed until a stable network of lenticular bubbles is established on the grain faces. An irradiation-induced

resolution process both delays the onset of release and modifies the eventual gas release rate.

The arrival rate of stable gas atoms at grain edge bubbles is employed to calculate the rate of interlinkage of these bubbles and the results of numerical finite difference surface diffusion calculations are invoked to evaluate the rate of collapse of interconnected tunnels. As the grain-edge tunnels grow, the collapse process eventually results in grain-corner porosity and similar arguments are used to evaluate the effective grain corner swelling rate.

The aperiodic opening and closing of the grain-edge tunnel network is considered as a system of taps linking a system of reservoirs. The passage of unstable gas atoms from the interior to the exterior of the fuel is delayed by the "aperiodic queueing" and the release mechanism may be viewed as an effective diffusion process through a polygranular fuel aggregate.

The model predictions compare very favourably with the experimental results of Turnbull and Friskney [12] for the release of I^{131} , I^{133} , Xe^{133} , Xe^{138} and Kr^{88} from spherical compacts of 1.46%-enriched stoichiometric UO_2 . The results obtained are independent of time step length, and calculations with temperature variation of $\pm 25^\circ C$ and rating deviations of $\pm 5\%$ from the documented fuel history suggests that any discrepancies between model and experiment must arise from other causes. It is considered that the main cause lies in uncertainties in the fission-gas and unstable fission-product diffusion coefficients. Following this conclusion, it is recommended that the experiments be re-analysed using the present model, to yield revised estimates for the diffusion coefficients.

Acknowledgement

This paper is published by permission of the Central Electricity Generating Board.

Appendix 1

A1.1. The mean dwell time of atoms at grain corners

An atom arriving at a grain corner will only be trapped there if the porosity along each of the four edges leading away from the corner is closed. In any time cycle of length $t_0 + t_c$ the edges can always be labelled (1) to (4) in order of being open, as indicated in fig. 22. In this way there are possible four periods in each cycle when all four tunnels are closed, signified in

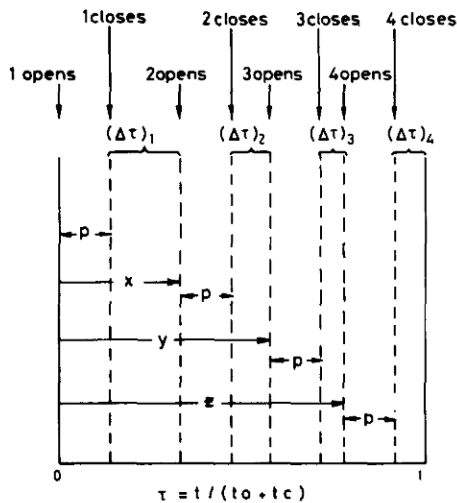


Fig. 22. The division of time into periods when a corner is completely sealed off ($\Delta\tau_i$, $i=1-4$) and periods when it is connected to surrounding corners—Appendix 1.

terms of the normalised time $\tau = t / (t_0 + t_c)$ by $\Delta\tau_i$ ($i=1-4$) in the diagram. Considering firstly $\Delta\tau_1$, the duration of this period is $x - p$, and if the gas atoms arrive at the corner, either by direct diffusion or by way of the tunnel network, at a constant rate B' , the total reduced time spent by gas atoms on that corner during the period is $B'(x - p)^2/2$.

In a total of

$$N_c = \int_0^1 dx \int_x^1 dy \int_y^1 dz = 1/6 \quad (A1)$$

possible configurations, the total time spent in periods $\Delta\tau_1$ is thus

$$\sigma_1 = \frac{B'}{2} (t_0 + t_c)^2 \int_p^1 (x - p)^2 dx \int_x^1 dy \int_y^1 dz. \quad (A2)$$

Similarly the total times spent in periods $\Delta\tau_2$, $\Delta\tau_3$ and $\Delta\tau_4$ may be written respectively

$$\left. \begin{aligned} \sigma_2 &= \frac{B'}{2} (t_0 + t_c)^2 \int_0^{1-p} dx \int_{x+p}^1 (y - x - p)^2 dy \int_y^1 dz \\ \sigma_3 &= \frac{B'}{2} (t_0 + t_c)^2 \int_0^{1-p} dx \int_x^1 dy \int_{y+p}^1 (z - y - p)^2 dz \\ \sigma_4 &= \frac{B'}{2} (t_0 + t_c)^2 \int_0^{1-p} dx \int_x^{1-p} dy \int_y^{1-p} (1 - z - p)^2 dz \end{aligned} \right\} \quad (A3)$$

where in each case the number of possible configurations is N_c given by eq. (A1).

The total dwell time of all atoms is $(\sigma_1 + \sigma_2 + \sigma_3 + \sigma_4)$

N_c and is $B'(1 - p)^5 (t_0 + t_c)^2/5$ and the number of atoms which have arrived at the corner during these closed periods is given by

$$n = B'(t_0 + t_c)[I_1 + I_2 + I_3 + I_4]/N_c, \quad (A4)$$

where

$$\left. \begin{aligned} I_1 &= \int_p^1 (x - p) dx \int_x^1 dy \int_y^1 dz \\ I_2 &= \int_0^{1-p} dx \int_{x+p}^1 (y - x - p) dy \int_y^1 dz \\ I_3 &= \int_0^{1-p} dx \int_x^{1-p} dy \int_{y+p}^1 (z - y - p) dz \\ I_4 &= \int_0^{1-p} dx \int_x^{1-p} dy \int_y^{1-p} (1 - z - p) dz \end{aligned} \right\} \quad (A5)$$

Evaluating these integrals yields

$$n = B'(t_0 + t_c)(1 - p)^4 \quad (A6)$$

and the average dwell time t per atom is clearly the total dwell time for all atoms divided by the number of atoms delayed hence

$$\bar{t} = (1 - p)(t_0 + t_c)/5 = t_c/5 \quad (A7)$$

and the effective jump frequency $\nu = \bar{t}^{-1}$.

A1.2. The mean jump distance along the interconnected porosity network

When a grain corner is open the probabilities of a gas atom penetrating 1, 2, 3 and N edges are respectively

$$1, \quad 1 - (1 - p)^3, \quad [1 - (1 - p)^3]^2$$

$$\text{and } [1 - (1 - p)^3]^{N-1}.$$

Thus the fraction of gas atoms contained within a single corner before its becoming open and penetrating N edges may be shown to be

$$(1 - p)^3 \langle 1 - (1 - p)^3 \rangle^{N-1}.$$

Since a group of gas atoms diffusing into a volume consisting of N edge lengths will move through a mean square distance $Nl^2/2$ the average number of edge lengths squared traversed by any gas atom per jump in an infinite polycrystal is

$$\frac{1}{2} \sum_{N=1}^{\infty} N(1 - p)^3 \langle 1 - (1 - p)^3 \rangle^{N-1} = 1/2(1 - p)^3.$$

Since each jump can be in a more or less random direction the root mean square distance transversed

through the polycrystal in making this jump is

$$\sqrt{d^2} = l/(1-p)^{3/2}\sqrt{2}$$

and the effective diffusion coefficient is

$$D_{\text{eff}} = \frac{1}{6} \nu d^2 = 5l^2/12t_c(1-p)^3.$$

A1.3. The mean time between complete corner re-opening

When the grain-edge tunnel radius is such that pinch off occurs in the edge centre it is unlikely that all four edges will seal simultaneously. The time taken to inflate a corner bubble to interlinkage is t_c but this period commences from the point when all four edges have sealed. If the origin of fig. 8 is redefined to be at the start of period $\Delta\tau_1$ then it is clear that all four tunnels are simultaneously closed at the start of $\Delta\tau_4$. This time is $z(t_0 + t_c)$ and hence the average delay in closing all four tunnels is

$$\frac{t_0 + t_c}{N_c} \int_0^1 dx \int_x^1 dy \int_y^1 zdz = \frac{3}{4}(t_0 + t_c).$$

Therefore on average the time between the first tunnel pinching off and the corner bubble re-opening is $t_c + \frac{3}{4}(t_0 + t_c)$ since re-inflation cannot commence until all four tunnels are sealed.

Appendix 2. Geometrical relationships for porosity

The volume and surface areas of the various bubbles described in the text are calculated by multiplying the volume (or area) of a sphere of the same radius of curvature by a correction factor which depends on the semidihedral angle θ . Most of the results which follow originate from the work of Clemm and Fisher [36].

The working definitions used here are

$$v = \frac{4}{3}\pi r^3 f_i(\theta), \\ A = 4\pi r^2 f_{ai}(\theta), \text{ and} \\ k = \cos \theta.$$
(A8)

(i) Grain face lenticular porosity

These bubbles are formed by the intersection of two spherical surfaces and hence have a circular projection. The angle at which the curved surfaces meet is 2θ , fig. 23a, and the projected circular radius is $r \sin \theta$. The correction factor for the volume is

$$f_f(\theta) = 1 - 3k/2 + k^3/2.$$
(A9)

(ii) Triangulated tunnel

These are cylindrical tunnels along grain edges formed by the intersecting of three cylinders such that the surfaces meet at 2θ fig. 23b. Since the profile is uniform the volume per unit length is [37]:

$$v = \pi r^2 f_T(\theta),$$
(A10)

where

$$f_T(\theta) = \frac{3}{\pi} \left\{ \theta - \frac{\pi}{6} - 2 \cos \theta \sin \left(\theta - \frac{\pi}{6} \right) / \sqrt{3} \right\}.$$

(iii) Triangulated grain edge bubbles

These are formed from the intersection of three spherical surfaces such that the surfaces meet at 2θ . In cross-section they appear as fig. 23b, whilst in profile they are cigar shaped as in fig. 23c.

The dimensions are

$$\left. \begin{aligned} l_b &= \left\{ 1 - \frac{4k^2}{3} \right\}^{1/2} r \\ \psi &= \arccos \left\{ \frac{2k}{\sqrt{3}} \right\} \end{aligned} \right\}$$
(A11)

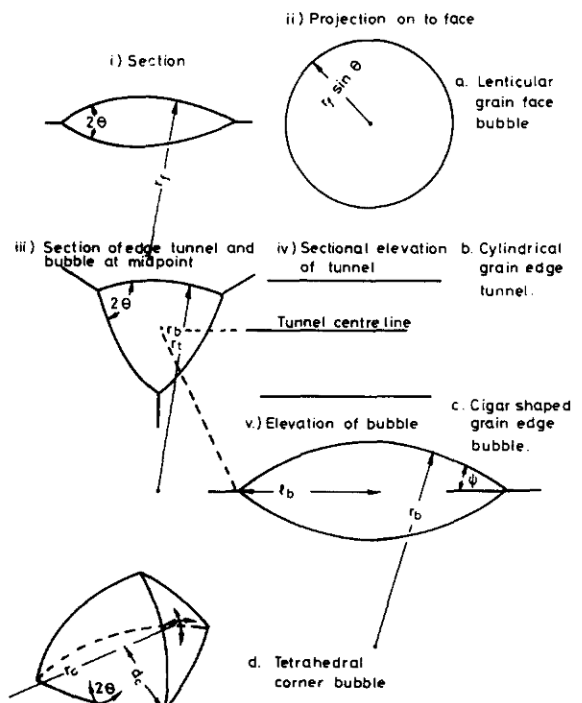


Fig. 23. Shapes of grain-face, grain-edge and corner porosity discussed in Appendix 2.

and the volume correction factor is

$$f_c(\theta) = \frac{3}{2\pi} \left\{ \pi - 2\alpha + \frac{k^2}{3} (3 - 4k^2)^{1/2} - \beta k (3 - k^2) \right\}, \quad (\text{A12})$$

where

$$\alpha = \arcsin \left\{ \frac{1}{2(1 - k^2)^{1/2}} \right\},$$

$$\beta = \arccos \left\{ \frac{k}{[3(1 - k^2)]^{1/2}} \right\}.$$

(iv) Grain-corner bubble

These are constructed from the intersection of four spherical surfaces with the surfaces meeting at 2θ , fig. 23d.

The volume correction factor is

$$f_c(\theta) = \frac{3}{2\pi} \left\{ 4 \left(\frac{\pi}{3} - \delta \right) + kK \left\{ \left(1 - k^2 - \frac{K^2}{4} \right)^{1/2} - \frac{K}{\sqrt{8}} \right\} - 2k\phi(3 - k^2) \right\}, \quad (\text{A13})$$

where

$$K = \frac{4}{3} \left(\frac{3}{2} - 2k^2 \right)^{1/2} - \frac{2k}{3},$$

$$\phi = \arcsin \left\{ \frac{K}{2(1 - k^2)^{1/2}} \right\},$$

$$\delta = \arccos \left\{ \frac{\sqrt{2} - k(3 - K^2)^{1/2}}{K(1 - k^2)^{1/2}} \right\}.$$

The surface area correction factor is

$$f_{AC}(\theta) = \frac{6}{\pi} \left\{ \frac{\pi}{3} - k\phi - \delta \right\}, \quad (\text{A14})$$

and the distance from the centre of the bubble to each vertex is

$$d_c = \frac{3r \sin E}{\sqrt{8}}, \quad (\text{A15})$$

where

$$E = \arccos \left\{ \frac{2k}{\sqrt{3}} \right\} - \arcsin \left(\frac{1}{3} \right).$$

(v) The variation of each of these quantities is shown in table 4 for various values of semi-dihedral angle. As

Table 4

θ	$f_i(\theta)$	$f_T(\theta)$	$f_c(\theta)$	$f_c(\theta)$	$f_{AC}(\theta)$	d_c/r
35	0.046	0.0046	0.0012	—	—	—
40	0.076	0.0199	0.0077	—	0.0103	0.1537
45	0.116	0.0482	0.0232	0.0059	0.041	0.2887
50	0.168	0.0909	0.0517	0.0208	0.090	0.4077
55	0.234	0.1494	0.0964	0.0507	0.155	0.5152
60	0.312	0.224	0.160	0.101	0.237	0.6124
65	0.404	0.316	0.246	0.175	0.333	0.7003
70	0.507	0.424	0.354	0.278	0.443	0.7888
75	0.620	0.548	0.485	0.413	0.565	0.8489
90	1.0	1.0	1.0	1.0	1.0	1.0

expected each approaches unity for $\theta \rightarrow \pi/2$ since in this case the shape is a complete sphere. The sensitivity around $\theta = 50^\circ$ is also of interest, a 5° change either way results in a factor of two in the volume of the bubbles.

Appendix 3. Fuel swelling after tunnel interlinkage ($\Delta V/V > 6\%$)

The swelling due to gas bubbles is given by

$$\frac{\Delta V}{V} = \left\{ \frac{\Delta V}{V} \right\}_0 + G\Delta B, \quad (\text{A16})$$

where $\langle \Delta V/V \rangle_0$ is the swelling at the start of the period, ΔB is the duration of the period in units of % Burnup and G is an empirical parameter deduced from AGR fuel post irradiation examinations. To convert ΔB to real time units, 1% burnup is equivalent to 9240 MWD/Te *. Therefore we may rewrite eq. (A16) in terms of the fuel rating W_r (W/g)

$$\frac{\Delta V}{V} = \left\{ \frac{\Delta V}{V} \right\}_0 + \frac{W_r \Delta t}{9240}, \quad (\text{A17})$$

and Δt is the period length in seconds.

The values of G are for a temperature T_c °C

$$\begin{aligned} T_c < 1000^\circ\text{C}: \quad G = 0.0, \\ 1000^\circ\text{C} < T_c < 1950^\circ\text{C}: \quad G = (T_c - 1000)/9500, \\ 1950^\circ\text{C} < T_c < 2500^\circ\text{C}: \quad G = 0.4014 - 1.545 \times 10^{-4} T_c, \\ 2500^\circ\text{C} < T_c: \quad G = 1.5 \times 10^{-2}. \end{aligned}$$

A limit is placed on the total swelling $\Delta V/V$ for the various temperature ranges and beyond these no extra swelling occurs.

$$1000 < T_c < 1950: \quad \left\{ \frac{\Delta V}{V} \right\}_{\max} = 0.2,$$

* Megawatt days per tonne (Uranium).

$$\begin{aligned}
 1950 < T_c < 2000: \quad & \left\{ \frac{\Delta V}{V} \right\}_{\max} = 4.1 - 2.0 \times 10^{-3} T_c, \\
 2000 < T_c < 2500: \quad & \left\{ \frac{\Delta V}{V} \right\}_{\max} = 0.46 - 1.8 \times 10^{-4} T_c, \\
 2500 < T_c: \quad & \left\{ \frac{\Delta V}{V} \right\}_{\max} = 1.0.
 \end{aligned}$$

Appendix 4. The irradiation history calculated by Cordall [54] for the Turnbull and Friskney [12] experiments

Duration (days)	Temperature (°C)	Rating (W/g)
0.93	68.00	12.26
23.00	1420.00	12.26
3.74	40.00	0.01
1.21	680.00	12.17
23.00	1400.00	12.17
3.90	40.00	0.01
0.95	680.00	10.94
23.10	1425.00	10.94
3.88	40.00	0.01
5.95	680.00	11.97
17.00	1430.00	11.97
4.88	40.00	0.61
1.00	750.00	17.99
23.10	1430.00	17.99
3.88	40.00	0.01
3.05	750.00	17.69
18.50	1350.00	17.69
3.83	40.00	0.01
1.06	750.00	17.39
21.30	1450.00	17.39
3.92	40.00	0.01
1.10	750.00	17.07
23.00	1450.00	17.07
4.01	40.00	0.01
4.94	750.00	16.71
19.00	1287.00	16.71
2.94	40.00	0.01
1.03	750.00	16.33
25.00	1287.00	16.33
3.77	40.00	0.01
3.18	750.00	15.97
20.00	1287.00	15.97
3.86	40.00	0.01
4.18	750.00	15.61
20.00	1298.00	15.61
3.85	40.00	0.01
0.72	700.00	15.26
21.60	1144.00	15.26

Appendix 5. List of symbols

- a^0 equivalent spherical grain radius at zero swelling (m),
- a spherical grain radius (m),
- a_1 tunnel pinch-off calibration proportionality,
- a_2 bubble spacing parameter after tunnel pinch-off,
- α number of new intragranular bubbles created per fission,
- α^i scaling factors for unstable/stable atom diffusion coefficients,
- A poly-granular aggregate radius (m), dummy variable in incubation equation,
- b Van der Waals volume (m^3/atom),
- b_ν resolution probability from grain face bubbles (s^{-1}),
- b' resolution probability from grain face intragranular bubbles (s^{-1}),
- β generation rate of stable fission gas atoms ($\text{atoms}/\text{m}^3\text{s}$),
- β_u generation rate of unstable gas atoms ($\text{atoms}/\text{m}^3\text{s}$),
- β_{eff} effective generation rate of unstable fission gas atoms after allowance for decay at grain face bubbles has been made ($\text{atoms}/\text{m}^3\text{s}$),
- c gas concentration (atoms/m^3)
- c_δ gas atom concentration at resolution depth (atoms/m^3),
- c^0 initial gas atom concentration at start ($t = 0$) of irradiation (atoms/m^3),
- \tilde{c}^0 initial gas atom concentration at start ($t = t^0$) of present irradiation period (atoms/m^3),
- C_B^{tot} total concentration of intragranular gas bubbles (m^{-3}),
- $C_B(R)$ distribution function for size of intragranular gas bubbles (m^{-3}),
- d_c distance from centre to vertex of tetrahedral grain corner bubble (m),
- δ resolution layer depth from grain face (m),
- D stable gas atom diffusion coefficient (m^2/s),
- D' stable gas atom diffusion coefficient after attenuation at intragranular bubbles (m^2/s),
- D_u unstable gas atom diffusion coefficient ($= \alpha' D$, m^2/s),
- D_s surface diffusion coefficient (m^2/s),
- D_{eff} effective diffusion coefficient for atoms travelling via intermittently open tunnel network (m^2/s),
- D_V, D_I vacancy and interstitial diffusivities (m^2/s),
- f_A “annealing” Booth fractional release of previously generated fission products,

f_c	"current" Booth fractional release,	\hat{R}_u	release rate for unstables (atoms/m ³ s),
$f_f(\theta)$	geometric factor relating volume of grain-face bubble to sphere,	R_0	incubation radius for intragranular bubbles (m),
$f_e(\theta)$	geometric factor relating volume of grain-edge bubble to sphere,	R^*	most probable radius for intragranular bubbles (m),
$f_t(\theta)$	geometric factor relating volume of grain-edge tunnel to cylinder,	\bar{R}	mean probable radius for intragranular bubbles (m),
$f_c(\theta)$	geometric factor relating volume of grain-corner bubble to sphere,	\bar{R}^n	n th moment of radius for intragranular bubbles (m),
f_b	fractional cover of grain faces by lenticular bubbles,	\dot{R}_f	arrival rate of atoms at grain faces (atoms/m ² s),
$f_{AC}(\theta)$	geometric factor relating surface area of grain-corner bubble to sphere,	\dot{R}_c	arrival rate of atoms at grain-corner bubbles (atoms/s),
F	fission rate (fission/m ³ s),	\dot{R}_e	arrival rate of atoms at unit length of grain edge before and after incubation (atoms/m s),
g	capture rate for gas atoms at intragranular bubbles (s ⁻¹),	s	atomic jump distance $\Omega^{-1/3}$ (m),
γ_{gb}	grain boundary surface energy (J/m ²),	s_g	swelling on grain face at saturation,
γ_{fs}	free surface energy (J/m ²),	$\Delta S/S$	fraction of grain boundary area occupied by tunnels,
j_v	vacancy jump frequency (s ⁻¹),	t	time (s),
k	Boltzmann constant (J/K, erg/K, eV/K),	t_c	coalescence time for bubbles (s),
k_a^2	$\alpha = I, V$; internal fixed sink strengths for interstitials and vacancies (m ⁻²),	t_{inc}	incubation time for grain face saturation (s),
K	point defect generation rate (s ⁻¹),	t_{gs}	delay time for unstables at grain-face bubbles (s),
l	grain edge length in TKD approximation (m),	t_0	pinch-off time for tunnel network (s),
l_f	range of fission fragment (m),	Δt	duration of irradiation period (s),
λ	decay constant (s ⁻¹),	τ_L	leakage time for atoms escaping via tunnel (s),
m	concentration of gas in intragranular bubbles (m ⁻³),	θ	semi-dihedral angle (degrees or radians),
v_c	venting rate of grain corner (s ⁻¹),	u	dummy time, variable in incubation equation,
N_f	areal density of gas atoms on grain faces (atoms/m ²),	$\Delta V/V$	fractional grain-edge and corner swelling,
N_f^{\max}	areal density of gas atoms on grain faces at saturation (atoms/m ²),	ω	dimensionless diffusion time (= Dt/a^2),
N_e^{\max}	number of gas atoms required to re-inflate a grain-edge bubble	W_R	fuel rating (W/g),
N_c^{\max}	number of gas atoms required to re-inflate a grain corner bubble,	γ'	fission yield for unstable atoms,
\dot{N}_f	arrival rate of gas atoms in grain edge tunnels prior to grain face saturation (atoms/m ² s),	Z_0	damage radius of fission fragment (m).
Ω	atomic volume (m ³),		
p	probability of finding grain-edge tunnel open,		
P_{ext}	external restraint pressure on fuel (unspecified),		
ϕ	areal density of gas atoms on grain face as a fraction of saturation density, (N_f/N_f^{\max}),		
ψ	total gas concentration in grain (m ⁻³ s ⁻¹),		
Q	quantity of gas released from grain (m ⁻³),		
r_b	radius of grain edge bubble (m),		
r_c	radius of grain corner bubble (m),		
r_f	radius of grain face bubble (m),		
r_{gf}	radius of grain face in toroid model (m),		
r_t	radius of grain edge triangulated tunnel (m),		

References

- [1] R. Hargreaves and D.A. Collins, J. Brit. Nucl. Energy Soc. 15 (1976) 311.
- [2] A.H. Booth, AECL Report No. 496 (1957).
- [3] M.V. Speight, Nucl. Sci. Engrg. 37 (1969) 180.
- [4] J.A. Turnbull, J. Nucl. Mater. 50 (1974) 63.
- [5] R.M. Cornell, Phil. Mag. 19 (1969) 539.
- [6] R.M. Cornell, J. Nucl. Mater. 38 (1971) 319.
- [7] J.A. Turnbull, J. Nucl. Mater. 38 (1971) 203.
- [8] M.V. Speight, J. Nucl. Mater. 38 (1971) 236.
- [9] A.J. Manley, UKAEA TRG Report 1681 (W) (1968).
- [10] M.O. Tucker and R.J. White, J. Nucl. Mater. 98 (1981) 157.
- [11] A.W. Schilling, TRG Report, 777 (W) (1963).
- [12] J.A. Turnbull and C.A. Friskney, J. Nucl. Mater. 71 (1978) 238.

- [13] C.A. Friskney and J.A. Turnbull, CEGB Report No. RD/B/N4217 (1978).
- [14] J.A. Turnbull, C.A. Friskney, J.R. Findlay, F.A. Johnson and A.J. Walter, CEGB Report No. RD/B/N4892 (1980).
- [15] D. Davies and G. Long, AERE Report No. 4347(1963).
- [16] A.D. Brailsford and R. Bullough, Proceedings of the Berkeley Conference, The Metals Society, (1973) p. 148.
- [17] P.T. Heald and M.V. Speight, Acta Metall. 23 (1975) 1389.
- [18] Hj. Matzke, J. de Physique Colloque C9, Supplement au no. 11-12 (1973) Tome 34.
- [19] J.A. Turnbull, Radiation Effects 53 (1980) 243.
- [20] T.S. Noggle and J.O. Steigler, J. Appl. Phys. 31 (1960) 2199.
- [21] C. Baker, J. Nucl. Mater. 66 (1977) 283.
- [22] F.S. Ham, J. Phys. Chem. Solids 6 (1958) 335.
- [23] G.L. Reynolds, W. Beeré and P.T. Sawbridge, J. Nucl. Mater. 41 (1971) 112.
- [24] J.C. Killeen, Private communication (1981).
- [25] D.R. Olander, Fundamental Aspects of Nuclear Reactor Fuel Elements TID-26711-P1-ERDA (1976).
- [26] D. Dowling, R.J. White and M.O. Tucker, J. Nucl. Mater. 110 (1982) 37.
- [27] R.J. White, D. Dowling and M.O. Tucker, to be published (1982).
- [28] C. Jefferies and M.O. Tucker, to be published (1982).
- [29] M.H. Wood and J.R. Matthews, J. Nucl. Mater. 89 (1980) 53.
- [30] J.R. Matthews and M.H. Wood, Nucl. Engrg. Des. 56 (1980) 439.
- [31] A.H. Booth, AECL Report DCI-27 (1957).
- [32] H.S. Carslaw and J.C. Jaeger, Conduction of heat in Solids, 2nd ed. (Oxford University Press (1960).
- [33] R.J. White and M.O. Tucker, Unpublished work (1980).
- [34] M.O. Tucker, J. Nucl. Mater. 89 (1979) 199.
- [35] M.O. Tucker, J. Nucl. Mater. 75 (1978) 782.
- [36] P.J. Clemm and J.C. Fisher, Acta Metall. 3 (1955) 70.
- [37] M.O. Tucker and J.A. Turnbull, Proc. Roy. Soc. A343 (1975) 299.
- [38] J.A. Turnbull and M.O. Tucker, Phil. Mag. 30 (1974) 47.
- [39] P.J. Rinous, M.O. Tucker and A.G. Crocker, Proc. Roy. Soc. A382 (1982) 201.
- [40] M.O. Tucker and R.J. White, J. Nucl. Mater. 87 (1979) 1.
- [41] M.O. Tucker and R.J. White, to be published (1982).
- [42] M.O. Tucker and R.J. White, Res. Mechanica 1 (1980) 21.
- [43] A.W. Schilling, Unpublished work (1964).
- [44] S. Katcoff, Nucleonics 18 (1960) 201.
- [45] E.A.C. Crouch, Atomic Data and Nuclear Data Tables 19 (1977) 417.
- [46] G.L. Reynolds, J. Nucl. Mater. 24 (1967) 69.
- [47] E.N. Hodkin and M.G. Nicholas, J. Nucl. Mater. 47 (1973) 23.
- [48] P.S. Maiya, J. Nucl. Mater. 40 (1971) 57.
- [49] W.W. Mullins, J. Appl. Phys. 28 (1957) 333.
- [50] W.W. Mullins, J. Appl. Phys. 30 (1959) 77.
- [51] E.N. Hodkin and M.G. Nicholas, J. Nucl. Mater. 67 (1977) 171.
- [52] P. Nikolopoulous, S. Nazarés and F. Thümmler, J. Nucl. Mater. 71 (1977) 68.
- [53] P. Nikolopoulous, S. Nazarés and F. Thümmler, J. Nucl. Mater. 78 (1978) 213.
- [54] D. Cordall, Private communication (1980).
- [55] M.O. Tucker and J.A. Turnbull, J. Nucl. Mater. 83 (1979) 278.